JCB

Tools

Imaging of native transcription factors and histone phosphorylation at high resolution in live cells

Sascha Conic,[1,2,3,4] Dominique Desplancq,[5] Alexia Ferrand,[6] Veronique Fischer,[1,2,3,4] Vincent Heyer,[1,2,3,4] Bernardo Reina San Martin,[1,2,3,4] Julien Pontabry,[1,2,3,4,8] Mustapha Oulad-Abdelghani,[1,2,3,4] Kishore Babu N.,[9] Graham D. Wright,[7] Nacho Molina,[1,2,3,4] Etienne Weiss,[5] and László Tora[1,2,3,4,9]

[1]Institut de Génétique et de Biologie Moléculaire et Cellulaire, [2]Centre National de la Recherche Scientifique, UMR7104, [3]Institut National de la Santé et de la Recherche Médicale, U964, [4]Université de Strasbourg, and [5]Institut de Recherche de l'ESBS, UMR 7242, Illkirch, France
[6]Imaging Core Facility, Biozentrum, University of Basel, Basel, Switzerland
[7]Institute of Medical Biology, A*STAR, Singapore, Singapore
[8]Helmholtz Zentrum München, Deutsches Forschungszentrum für Gesundheit und Umwelt (GmbH), Institute of Epigenetics and Stem Cells, München, Germany
[9]School of Biological Sciences, Nanyang Technological University, Singapore

Fluorescent labeling of endogenous proteins for live-cell imaging without exogenous expression of tagged proteins or genetic manipulations has not been routinely possible. We describe a simple versatile antibody-based imaging approach (VANIMA) for the precise localization and tracking of endogenous nuclear factors. Our protocol can be implemented in every laboratory allowing the efficient and nonharmful delivery of organic dye-conjugated antibodies, or antibody fragments, into different metazoan cell types. Live-cell imaging permits following the labeled probes bound to their endogenous targets. By using conventional and super-resolution imaging we show dynamic changes in the distribution of several nuclear transcription factors (i.e., RNA polymerase II or TAF10), and specific phosphorylated histones (γH2AX), upon distinct biological stimuli at the nanometer scale. Hence, considering the large panel of available antibodies and the simplicity of their implementation, VANIMA can be used to uncover novel biological information based on the dynamic behavior of transcription factors or posttranslational modifications in the nucleus of single live cells.

Introduction

Although transgenic or overexpression-based approaches are well-established to follow the spatiotemporal localization (and in rare cases the activity) of different intracellular factors in real time, the detection of endogenous cellular factors in live cells is not yet routinely possible. Visualization of cellular structures and processes is typically performed by using immunofluorescence (IF) labeling of fixed cells or exogenous overexpression of fluorescently tagged proteins (FTPs) in live cells. In IF, specific labeling of proteins is typically achieved by incubating chemically fixed and permeabilized cells with primary antibodies followed by specific secondary antibodies conjugated to fluorophores. Despite many variables (e.g., permeabilization efficiency, protein denaturation, access to epitopes, and antibody quality), IF is routinely used for visualizing targeted, but immobile, proteins in fixed cells and tissues (Schnell et al., 2012; Teves et al., 2016). On the other hand, imaging of nuclear proteins in living cells is often achieved through exogenous expression of the protein of interest fused to a fluorescent protein tag (FP; Ellenberg et al., 1999; Betzig et al., 2006; Schneider and Hackenberger, 2017) or knock-in of an FP tag coding cDNA at the endogenous loci by the CRI SPR/Cas9 technology to create an endogenous FTP (Ratz et al., 2015). Although FTPs have proven to be very powerful, the continually developing FPs are suboptimal, when compared with dyes, because of the relatively limited quantum yield and low photostability. In addition, FTPs do not always behave as their endogenous counterparts (because of the FP tag) and/or their elevated levels when exogenously overexpressed (Burgess et al., 2012).

It has been well established that the function of transcription factors and coactivator complexes involved in chromatin-dependent processes are tightly linked to their mobility and interactions with diverse posttranslational modifications (PTMs) in the nuclear environment (Snapp et al., 2003; Kimura, 2005; Hager et al., 2009; Cisse et al., 2013; Vosnakis et al., 2017). Our current understanding of transcription regulation dynamics is often based on approaches, called fluorescence recovery after photobleaching and florescence loss in photobleaching, in which fluorescently tagged factors in the nucleus, or a whole cellular compartment, are bleached and the fluorescence redistribution is followed over time in live cells (Kimura et al., 1999, 2002; Dundr et al., 2002; Kimura, 2005;

Correspondence to Etienne Weiss: etienne.weiss@unistra.fr; László Tora laszlo@igbmc.fr

The Rockefeller University Press
J. Cell Biol. Vol. 217 No. 4 1537–1552
https://doi.org/10.1083/jcb.201709153

Gorski et al., 2008; van Royen et al., 2011). Fluorescence correlation spectroscopy, is a microscopy technique where less than 200 molecules are measured, but also based on the detection and quantification of fluorescently tagged factors diffusing through a subfemtoliter observation volume (Macháň and Wohland, 2014). Moreover, single-particle tracking approaches combined with super resolution microscopy often rely also on protein tagging with FPs or photoactivable FPs (Beghin et al., 2017). Consequently, at present there is no simple approach to track accurately nontagged, native transcription factors or to detect the appearance and/or the disappearance of PTMs in the nuclear environment of living cells at high resolution. Thus, there is a demand for novel, powerful tools to gain insight in the dynamic behavior of endogenously expressed proteins in single live cells.

Fluorescently labeled antibodies poorly penetrate through the intact membranes of living cells, making it challenging to image intracellular endogenous proteins (Marschall et al., 2011). Methods have been described that attempted to overcome this through microinjection, osmotic lysis of pinocytic vesicles, loading with glass beads, or protein transfection by using various cationic lipids or polymers (Manders et al., 1999; Courtête et al., 2007; Röder et al., 2017). Recently, fluorescent labeling of proteins inside live mammalian cells has been achieved by using streptolysin O, a bacterial toxin, which creates pores in the cell membrane and allows the delivery of fluorescent probes (Teng et al., 2016). However, this method required additional steps to reseal the membrane pores. Many of these techniques require very specialized know-how and/or equipment, suffer from low efficiency, and/or are harmful for the cells. Significant effort has also been put into antibody engineering of single-chain variable (scFv) fragment antibodies, which can be expressed intracellularly as recombinant scFvs (intrabodies), but unfortunately many of these intrabodies have proven to be insoluble and aggregate in the reducing environment of the cytosol (Renaud et al., 2017). The delivery of nonlabeled mouse mAbs in human cells using electroporation and their subsequent detection in fixed cells has been described (Berglund and Starkey, 1989; Chakrabarti et al., 1989; Lukas et al., 1994; Freund et al., 2013; Marschall et al., 2014; Desplancq et al., 2016).

Because antibodies can be efficiently labeled with fluorophores by using conventional methods and reliably delivered into the cytoplasm by electroporation, we tested whether such probes, which do not need exogenous protein expression or genetic manipulations, can be used for the specific detection and tracking of endogenous nuclear factors in live cells. Here we describe a versatile antibody-based imaging approach (VANIMA) for conventional and super-resolution imaging and tracking of endogenous nuclear factors in live cells by means of fluorescently labeled antibodies or antibody fragments. Their intracytoplasmic delivery into cultured cells was achieved through a simple nontoxic and highly efficient electroporation step. By following the fate of these conventional and noninterfering probes in live cells, it was possible to uncover novel cell biological insights by tracking at nanometer scale native transcription factors (i.e., RNA polymerase II [Pol II], TATA binding protein [TBP], and TBP-associated factor 10 [TAF10]) and image the dynamics of phosphorylated histone H2AX.

Results

Proof of principle of VANIMA: Targeting RNA Pol II in single living cells

To visualize an endogenous nuclear target protein, we selected an mAb that was raised against the heptapeptide repeats present in the nonphosphorylated C-terminal domain (CTD) of the largest subunit (RPB1) of RNA Pol II, hereafter called anti-RPB1 mAb, which performed well in IF assays (Lebedeva et al., 2005). This mAb was first purified and randomly labeled with Alexa Fluor 488 fluorescent dye. Labeling efficiency calculations indicated that the anti-RPB1 mAb contained five to seven covalently linked dye molecules per mAb. To transduce the antibodies into cells, the cell membrane was shortly permeabilized by a brief electric shock with the use of a commercially available apparatus (see Materials and methods), enabling the antibodies to enter the cytoplasm. Once inside the living cells, the antibodies can be imaged by using various microscopy techniques. The labeled anti-RPB1 mAb was electroporated into a large variety of different mammalian or *Drosophila melanogaster* cell types with a delivery efficiency of ∼94–99% and a viability efficiency of 56–99% (Table S1). Approximately 6 h after electroporation, during which the cells attach to the culture dish, the labeled anti-RPB1 mAb was detected in the cytoplasm of human U2OS cells (Fig. 1 A and Video 1). Full-length mAbs are unable to enter the nucleus because of their large size (150 kD; Hayashi-Takanaka et al., 2011; Desplancq et al., 2016; Teng et al., 2016). However, interestingly, after ∼24 h the anti-RPB1 mAb-bound Alexa Fluor 488 signal was almost completely nuclear, indicating that the labeled anti-RPB1 mAb bound to newly synthesized target protein, RPB1, in the cytoplasm and was piggybacked into the nucleus (Fig. 1 A and Video 1). When we transduced 0.5, 1, 2, and 4 µg labeled anti-RPB1 mAb (corresponding to about between 5×10^4 and 4×10^5 antibody molecules per cell; Freund et al., 2013), we observed that with 4 µg electroporated anti-RPB1–Alexa Fluor 488 mAb the nuclear signal became saturated because at this concentration of mAb a cytoplasmic signal persisted 24 h after the transduction (Fig. 1 B). This indicated that with $\sim 4 \times 10^5$ molecules of antibodies per cell we have saturated all the available binding sites on the CTDs of RPB1 and that with between 2×10^5 and 4×10^5 molecules of antibodies per cell most of the endogenous Pol II molecules were labeled (Fig. 1 B). The fact that U2OS cells contain $\sim 9 \times 10^4$ molecules of Pol II (Zhao et al., 2014) further suggests that each RPB1 CTD may be bound by ∼2–4 molecules of anti-RPB1 mAb. Moreover, as each mAb is labeled with ∼5–7 molecules of dye, it means that each Pol II molecule can be visualized by 10–28 molecules of dye.

To test whether the electroporated anti-RPB1 mAb that was piggybacked to the nucleus by RPB1 (Fig. 1 A and Video 1) would stay bound to its target, we transduced U2OS cells with 0.5, 2, and 4 µg anti-RPB1 mAb. 24 h after transduction we lysed the cells, prepared whole-cell extracts, mixed the antibody-containing cell extracts with protein G Dynabeads, and tested whether the extracted anti-RPB1 mAb would still be bound to RPB1 (Fig. 1 C). Our experiment shows that the electroporated labeled anti-RPB1 mAb remains bound under these conditions and that all the cellular Pol II can be bound by the transduced labeled antibody.

As a large portion of Pol II is bound to the chromatin during transcription in the cells (Kimura et al., 1999), we tested whether the Alexa Fluor 488–labeled anti-RPB1-mAb would

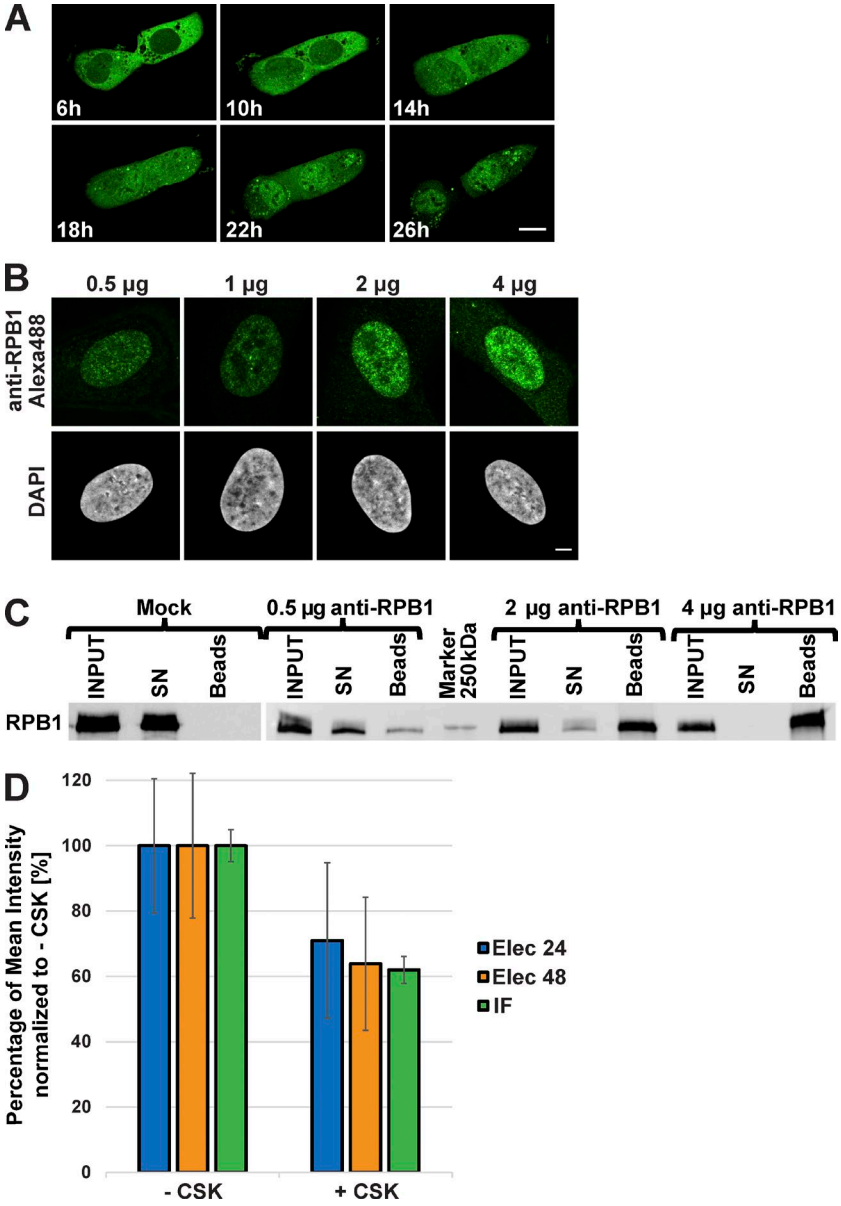

Figure 1. **Behavior of the anti-RPB1 mAb in U2OS cells. (A)** After transduction with Alexa Fluor 488–labeled anti-RPB1 antibodies, cells were imaged after 6 h of incubation and then every hour over a period of 20 h (see Video 1 for all time points). Bar, 15 µm. **(B)** Increasing amounts of Alexa Fluor 488–labeled anti-RPB1 mAb were transduced in U2OS cells and fixed 24 h after electroporation. A typical nucleus recorded in each case after counterstaining with DAPI is shown. Bar, 5 µm. **(C)** Binding capacity of anti-RPB1 mAb in U2OS cells. Cells were electroporated with 0 (mock), 0.5, 2, and 4 µg anti-RPB1 mAb and whole-cell extracts prepared 24 h after transduction (INP UT) were mixed with protein G beads. Bound and unbound material was analyzed by Western blotting. The blot shows the fraction of antibody-bound Pol II molecules adsorbed on the beads (beads) or left in the supernatant (SN), and detected with a secondary antibody. **(D)** After transduction with Alexa Fluor 488–labeled anti-RPB1 mAb (2 µg), cells were treated with or without CSK buffer. The histogram shows the mean fluorescence intensity of the nucleus of nontreated (–CSK) and CSK-treated (+CSK) cells 24 h (Elec 24h) or 48 h (Elec 48h) after electroporation. A classical anti-RPB1 mAb IF experiment was performed as additional control (IF). The +CSK signal is represented as the percentage of the mean intensity of the –CSK signal. Error bars represent the SD obtained with 10 recorded cells for each condition. All images were acquired by confocal microscopy on one single z plane.

also stay bound to the chromatin associated Pol II. To this end, 24 or 48 h after transduction anti-RPB1–Alexa Fluor 488 mAb–transduced cells were treated, or not, with a mixture of detergent and sucrose known as cytoskeleton (CSK) buffer, which is widely used to release soluble proteins from cells, including the nucleus (Cramer and Mitchison, 1995). Cells were then fixed, and the Alexa Fluor 488 signal was quantified from nontreated and CSK-treated cells 24 and 48 h after transduction. As a control, a classical anti-RPB1 mAb IF staining was performed. The quantification of IF detection of Pol II shows that in CSK-treated samples ∼60–70% of the total Pol II signal is bound to the chromatin. In agreement, the quantification of the electroporated anti-RPB1–Alexa Fluor 488 mAb signal indicated the presence of similar fraction of chromatin-bound endogenous Pol II (Fig. 1 D). These results further indicate that the transduced labeled anti-RPB1 mAb can bind to transcribing Pol II on the chromatin and that the electroporated mAb stays bound to its target during 48 h. These specific mAb-binding characteristics in cells suggest that VANIMA can be used for live-cell imaging experiments to characterize the behavior of transcription factors.

Imaging of several endogenous nuclear antigens with VANIMA

To further evidence the usefulness of the approach for imaging a range of nuclear factors, we have compared different transduced labeled mAbs (150 kD) with their corresponding Fab fragments (50 kD), because Fabs can freely enter the nuclei of cells (Hayashi-Takanaka et al., 2011). In these comparisons, different mAbs or Fabs were used, which were raised against different transcription factors (such as RBP1/Pol II, TBP, and TAF10). Our comparisons show that the labeled mAbs or their corresponding labeled Fab fragments perform similarly to label the endogenous transcription factors (Fig. 2, A and B; and Fig. S1 A). Importantly, labeled Fab fragments raised against nuclear proteins are reaching the nucleus 6 h after electroporation (Fig. S1 B), in contrast to mAbs that need ∼24–48 h to reach the nucleus by the piggybacking mechanism (Fig. 1 A).

Next, we verified whether the electroporated Alexa Fluor 488–labeled anti-TAF10 or anti-TBP mAbs would stay bound to their respective targets after electroporation and piggybacking in the nucleus. To this end cells were electroporated with in-

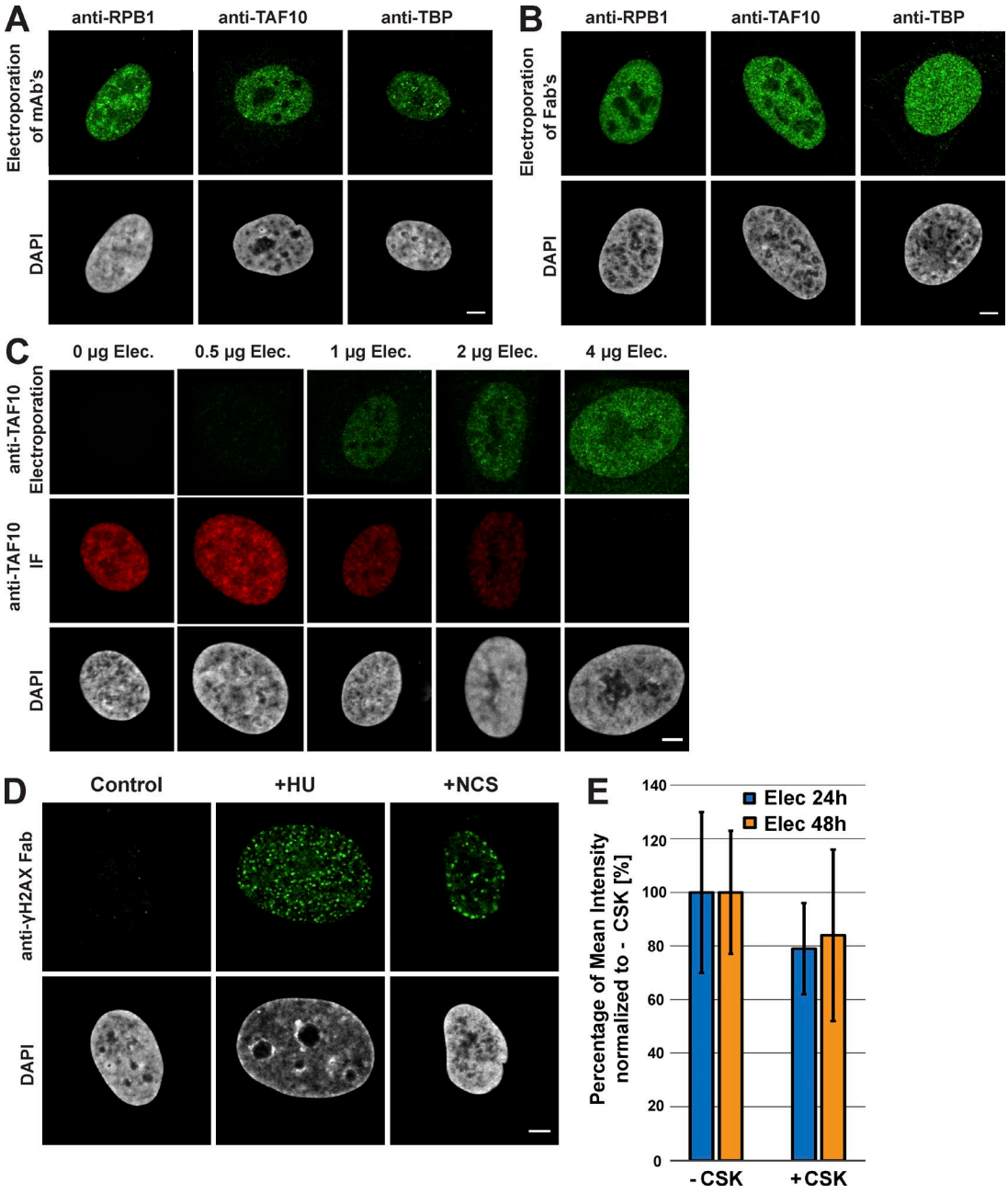

Figure 2. **Visualization of endogenous transcription factors and phosphorylated H2AX with VANIMA. (A)** The labeled mAbs binding specifically to the transcription factors RPB1, TAF10, and TBP were transduced in U2OS cells, and their localization in the cells was monitored by confocal microscopy 24 h after treatment. A single z plane is shown for each condition. The pictures represent a typical nucleus recorded in each case after fixation of the cells and subsequent counterstaining with DAPI. **(B)** Same as in A, except that the experiments were performed with the corresponding labeled Fab fragments. **(C)** Increasing amounts of Alexa Fluor 488–labeled anti-TAF10 mAb (green) were transduced in U2OS cells and fixed 24 h after electroporation (anti-TAF10 Electroporation). To verify binding of the antibody to TAF10, a competition assay was performed afterward by adding a constant amount (2 µg) of the same antibody but Alexa Fluor 568–labeled as IF antibody (red, anti-TAF10 IF; see also Fig. S1 C for quantification). DAPI staining is shown in gray. **(D)** The labeled Fab raised against γH2AX was transduced as in B, and its localization was recorded after treatment of the electroporated cells with either NCS (for 15 min) or HU (for 48 h). Control, nontreated cells. A typical nucleus is represented in each case. **(E)** After transduction with Alexa Fluor 488–labeled anti-γH2AX Fab (5 µg) and treatment with HU, cells were treated with or without CSK buffer before fixation. The histogram shows the mean fluorescence intensity of the nucleus of nontreated (–CSK) and CSK-treated (+CSK) cells 24 h (Elec 24h) or 48 h (Elec 48h) after electroporation. The +CSK signal is represented as the percentage of the mean intensity of the –CSK signal. Error bars represent the SD obtained with 10 recorded cells for each condition. Bars, 5 µm.

creasing amounts of Alexa Fluor 488–labeled antibodies, fixed 24 h after electroporation and subjected to IF with the same antibody but labeled with Alexa Fluor 568 dyes. These competition experiments and their quantifications show that when 10^6 cells were transduced with 4 µg antibodies, 24 h after electroporation the intracellular antibodies were still binding to all their target epitopes, as in these cells no significant IF signal could be detected (Fig. 2 C and Fig. S1 C).

It is noteworthy that electroporated mAbs raised against either a prokaryotic protein, and thus having no epitopes in the

human cell (such as the mAb against the maltose-binding protein [MBP]), or against a cytoplasmic target (such as the mAb against α-tubulin) do not enter in the nucleus (Fig. S1 D). All these results together suggest that both labeled mAbs and Fabs can be used for imaging nuclear antigens depending on the scientific question asked.

We also tested whether the transduced labeled antibodies would recognize chromatin-associated PTMs. To this end we used a Fab developed against γH2AX that is often considered a marker of DNA double-strand breaks (Siddiqui et al., 2015; Fig. S1 E). The histone variant H2AX, which can replace conventional histone H2A in nucleosomes, becomes phosphorylated on serine 139 (called γH2AX) upon DNA double-strand breaks. Note that when an epitope is generated only in the nucleus, such as histone PTMs, only labeled Fabs are adequate to detect these targets. Anti-γH2AX mAb was generated, and the corresponding labeled Fabs were transduced in control cells and in cells in which DNA damage was induced by hydroxyurea (HU) or neocarzinostatin (NCS) treatments (Fig. 2 D). As expected, Alexa Fluor 488–labeled Fab fragments could enter the nuclei of the cells and bind the serine 139 phosphorylated H2AX foci in the HU- or NCS-treated cell nuclei (Fig. 2 D), demonstrating that the transduced Fabs can bind to PTMs in the chromatin of live-cell nuclei. Next, we verified whether the electroporated Alexa Fluor 488–labeled anti-γH2AX Fab would stay bound to chromatin after electroporation and diffusion to the nucleus. To this end, cells were electroporated with anti-γH2AX Fab and treated with HU 6 h later, and soluble proteins were extracted with the CSK buffer 24 or 48 h after treatment. Cells were then fixed and the Alexa Fluor 488 signal (Fig. 2 E). These experiments further indicate that almost all the labeled anti-γH2AX Fab stays bound to chromatin and that at the indicated time points almost no unbound Fab could be detected.

To ascertain that our endogenous nuclear protein labeling approach with the use of the described antibodies would not interfere at a detectable level with the function of the target or cellular functions, we performed a series of tests 24 and 48 h after mAb electroporation. To verify whether the anti-RPB1, -TBP, or -TAF10 would inhibit transcription, RNA was isolated from electroporated cells and subjected to RT-qPCR analyses by using primers to amplify unspliced, and therefore newly synthesized, premRNA from Pol II target genes. The primers were designed to amplify sequences from introns to exons for several Pol II–transcribed genes (Table S2). As controls, cells were either transduced with an antibody targeting the bacterial MBP, which has no expected target in the human cells and therefore should not inhibit transcription. Cells were also treated with α-amanitin at a concentration that would inhibit Pol II transcription but not that of Pol I and Pol III. Our results show that the anti-MBP antibody and the other three mAbs tested did not significantly inhibit premRNA transcription of the tested Pol II genes, although α-amanitin almost completely abolished the transcription of the Pol II genes (Fig. 3, A and B). Next, we measured the cell cycle progression and the cell proliferation/replication capabilities of the antibody electroporated cells (Fig. 3, C and D). Both quantifications show that cell cycle progression and cell proliferation were not inhibited by the electroporation of the anti-RPB1, -TBP, -TAF10, or -MBP antibodies. Furthermore, apoptosis tests indicated that transduced antibodies did not induce significant cell death 24 h after their electroporation (Fig. 3 E). In conclusion, a noninterfering mAb recognizing a nuclear transcription factor should be suitable for VANIMA if after transduction it is piggybacked in the nucleus. Fabs can freely diffuse in the cell and only accumulate in the nucleus after transduction if bound to the nuclear target. In addition, both mAbs and Fabs should not inhibit significantly premRNA transcription, cell cycle progression, cell proliferation, or induce apoptosis.

Comparison to existing labeling techniques

We have also compared VANIMA to existing labeling techniques, such as IF, ectopic expression of GFP-fused transcription factors, or CRISPR/Cas9 knock-in technology. When using VANIMA and IF (Fig. S2 A) in parallel experiments, we obtained identical results on fixed cells, except that our approach does not necessitate a fixation step for the accurate detection of the targets (compare Fig. 2 A and Fig. S2 A). When comparing the labeling with transduced antibodies to the ectopic expression (overexpression) using GFP fusions of transcription factors, we observed as previously published that exogenously expressed GFP-RPB1 or CFP-TAF10 does not efficiently reach the nucleus or is excluded from the nucleus, respectively, in contrast to the endogenous counterparts (Soutoglou et al., 2005; Boulon et al., 2010; Wild and Cramer, 2012; Fig. S2, B and C). Moreover, ectopically expressed GFP-TBP was nuclear but excluded from the nucleoli of the cells (Fig. S2, B and C), suggesting that GFP-TBP does not enter the nucleoli despite TBP involvement in Pol I transcription (Hernandez, 1993). In contrast, the antibody-labeling method revealed the expected behavior of the endogenous nuclear transcription factors (compare Fig. 2 and Fig. S2, B and C). To be able to compare VANIMA to cells where a fluorescent tag has been expressed from the endogenous locus in fusion with a transcription factor, we knocked-in a Venus tag in frame at the 5′ end of the *TAF10* locus in U2OS cells using the CRISPR/Cas9 methodology. Stable Venus-TAF10 expressing heterozygous U2OS clones were generated, and the fluorescence obtained from these cells was compared with U2OS cells that were simply transduced for 24 h with an anti-TAF10 mAb labeled with Alexa Fluor 488. The comparison shows that electroporated cells give a signal largely overlapping with that obtained in Venus-TAF10 expressing cells but that the labeled mAb-bound TAF10 signal is brighter than Venus-TAF10 signal when using a confocal microscope (Fig. S2, D and E).

Analysis of Pol II, TAF10, and γH2AX distribution in subnuclear structures by super-resolution microscopy

To obtain high-resolution images of endogenous proteins and PTMs, we used super-resolution microscopy (Betzig et al., 2006). To be able to carry out multichannel detection and live-cell imaging the target-bound labeled mAbs and Fabs were visualized by 3D structural illumination (3D-SIM) super-resolution microscopy at ∼110 nm xy and ∼300 nm z resolution first in fixed cells (Schermelleh et al., 2008). By using 3D-SIM, the labeled mAbs and Fabs allowed the detection of well-defined individual spots of different sizes in the nuclei of U2OS cells (Fig. 4, A and B; and Videos 2–4). In agreement with previous studies (Markaki et al., 2010), the detection of Pol II, TAF10, and TBP by 3D-SIM seemed to be excluded from DAPI dense regions (Fig. 4, A and B).

We measured the nuclear distribution of Pol II and TAF10 molecules labeled with anti-RPB1 mAb-Alexa Fluor 488 and anti-TAF10 mAb-Alexa Fluor 488, respectively, using 3D-SIM. To quantify the number and sizes of the observed foci, we pro-

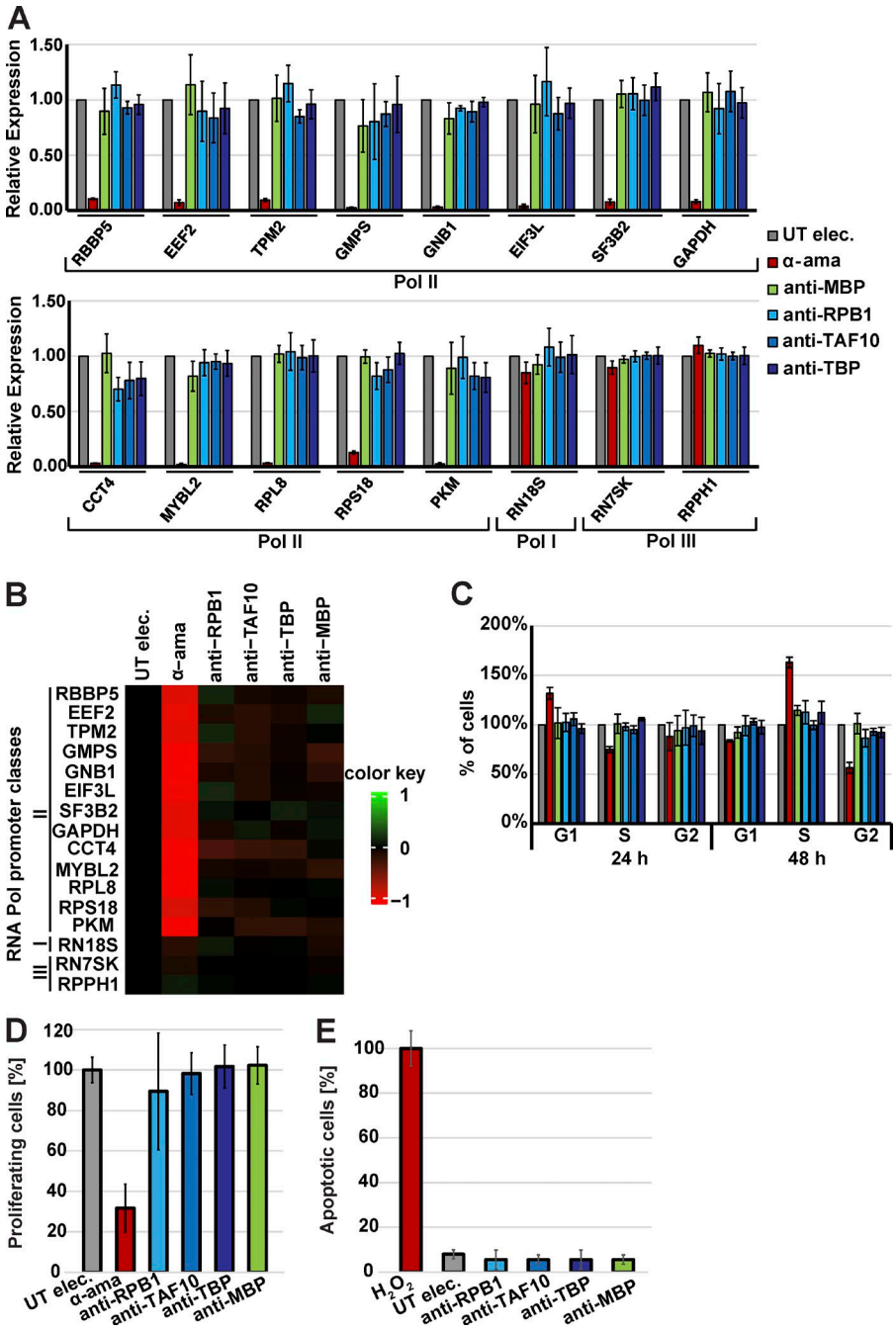

Figure 3. **The mAbs do not inhibit premRNA transcription, cell cycle progression, cell proliferation and do not induce apoptosis. (A)** U2OS cells electroporated but without antibodies (UT elec), electroporated and treated with α-amanitin (α-ama), electroporated with a control antibody binding to bacterial MBP (anti-MBP), or electroporated with the mAbs recognizing specifically RPB1, TAF10, or TBP (anti-RPB1, anti-TAF10, or anti-TBP). 24 h after electroporation, total RNA was isolated, and the expression of Pol I, Pol II, and Pol III genes was analyzed by RT-qPCR. Pol III transcripts were used for normalization. Newly synthesized RNA of the indicated genes was quantified with validated primer pairs (Table S2). The histograms correspond to the mean values obtained with three independent experiments. **(B)** The mean values of the three independent experiments shown in A are represented as a heatmap reflecting unchanged relative expression in black, up-regulation in green, and down-regulation in red. **(C)** U2OS cells were electroporated as in A, and cell cycle progression was monitored by propidium iodide staining and FACS analysis 24 or 48 h after electroporation. The cell cycle phases were normalized to cells electroporated without antibody. **(D)** U2OS cells were electroporated as in A, and their capacity of proliferation was monitored 24 h after transduction by EdU incorporation and FACS. The electroporated cells without the addition of antibody were used as control. The color code is as in A. **(E)** The cells were treated as in A, except an apoptosis test was performed 24 h after electroporation. Apoptosis induced by the addition of 10 µM H_2O_2 was taken as reference (100%). In each panel, the error bars represent the biological SD obtained from three independent replicates. UT, untreated cells.

cessed the images with Fiji/ImageJ and Matlab (see Materials and methods; Fig. 5, A–F). Our quantifications show that the size distribution of Pol II foci ranges from 10^{-3} µm^3 to ∼1.6 × 10^{-2} µm^3, with nearly 34% of the foci having the smallest volume (Fig. 5 A). TAF10 foci are in general smaller than those of Pol II, with 55% of the spots showing the smallest volume (Fig. 5 B). Interestingly, ∼3% of the Pol II foci are larger than 10^{-2} µm^3, whereas only 0.4% of the TAF10 foci fall in this category (Fig. 5 C). To investigate the biological significance of the observed spot sizes, we have inhibited transcription with 2 µM flavopiridol (Flavo), a known inhibitor of Pol II transcription elongation (Chao et al., 2000). 1-h Flavo treatment significantly reduced the RPB1 CTD phosphorylation by pTEFb (Vosnakis et al., 2017). Interestingly, the Flavo treatment reduced the volume of bigger Pol II foci and consequently increased about twofold the percentage of smaller Pol II spots between 10^{-3} and 4 × 10^{-3} µm^3 (Fig. 5 A). In addition, when the size distribution changes of the larger Pol II foci were considered (spots > 10^{-2} µm^3) after Flavo treatment, the percentage of larger Pol II foci was decreased by a factor of 4 (Fig. 5 C). In contrast, the size distribution of the TAF10 foci was not affected by Flavo treatment (Fig. 5, B and C). Interestingly, the total number of Pol II foci increased after Flavo treatment and was followed by a parallel decrease in the mean cluster size of Pol II foci. In agreement with a scenario in which the large Pol II foci would dissociate in several smaller spots, the total volume of labeled spots did not change (Fig. 5, D–F). In contrast, transcription elongation inhibition did not influence the total number, mean cluster size, or total volume of TAF10 foci (Fig. 5, D–F), indicating that the observed Pol II cluster size shift reflected in vivo

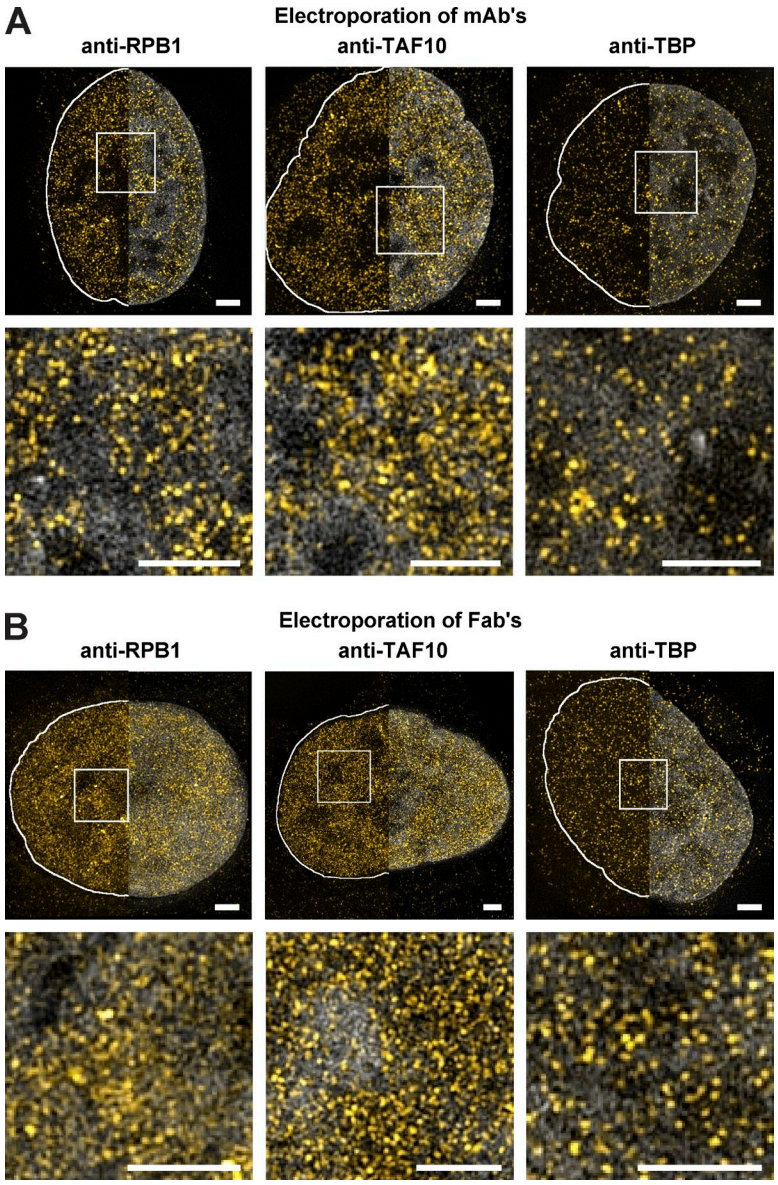

Figure 4. **Visualization of transcription factors with VANIMA by super-resolution microscopy. (A)** The labeled mAbs binding to the transcription factors RPB1, TAF10, and TBP (yellow) were transduced in U2OS cells, and their localization in the cells was monitored 24 h after transduction by 3D-SIM. The pictures show a typical nucleus recorded in each case after fixation and DAPI (gray) treatment (Videos 2–4). The Z maximum intensity projections of five slices show the labeled mAbs with (right half) or without (left half) DAPI counterstaining (gray). The solid white lines depict the nuclear contour. Bottom: Magnification of the white regions of interest, under the corresponding image. **(B)** The nuclei shown correspond to transduced U2OS cells as in A, except that transductions were performed with the corresponding labeled Fab fragments. Bars, 2 µm.

Pol II behavior changes after transcription inhibition. Using photobleaching techniques, it has been shown that, when transcription elongation is inhibited, total bound Pol II is released from the chromatin in general and becomes mobile (Kimura et al., 2002; Hieda et al., 2005; Vosnakis et al., 2017). Thus, our results show that when transcription elongation is inhibited by Flavo the larger Pol II foci dissociate, because Pol II molecules are released from these sites and become mobile.

To confirm the usefulness of delivered labeled antibodies in monitoring discrete nuclear structures labeled by various PTMs, we visualized and quantified the number of γH2AX-Fab–labeled foci before and after HU treatment using 3D-SIM (Fig. 6, A and B; and Videos 5 and 6). Our quantifications show that HU-induced DNA damage increased the number of γH2AX foci by ∼80-fold in treated cells (Fig. 6 B), suggesting that labeling with transduced Fab fragments allows precise analysis of chromatin modifications upon replication stress. The 3D-SIM experiments demonstrate that changes of individual nuclear structures, where transcription factors or specific PTMs are present or accumulate, can easily be revealed after different biological stimuli. Our approach can thus be used to uncover novel information concerning essential biological mechanisms.

Uncovering novel dynamic behaviors of transcription factors and PTM events by VANIMA by using high-resolution live-cell imaging

To test the adequacy of conventionally labeled antibodies for high-resolution live-cell imaging, we transduced anti-RPB1–Alexa Fluor 488 mAb into U2OS cells, and 24 h after transduction nuclei were imaged over a period of 2.5 h, taking images every 10 min by time-lapse confocal microscopy. These videos show that the larger Pol II spots/clusters, which can be easily detected at this resolution, are dynamically and constantly moving within the nucleus (Fig. 7 A and Video 7). To better visualize the shape and the movements of these larger Pol II clusters (ranging between 1 and 1.6×10^{-2} µm^3), they were imaged by using 3D-SIM over a short period. These live-cell measurements show that the larger Pol II-labeled foci are dynamic and are constantly associating and dissociating over time (Fig. 7 B and Video 8). In agreement with our nascent transcription ex-

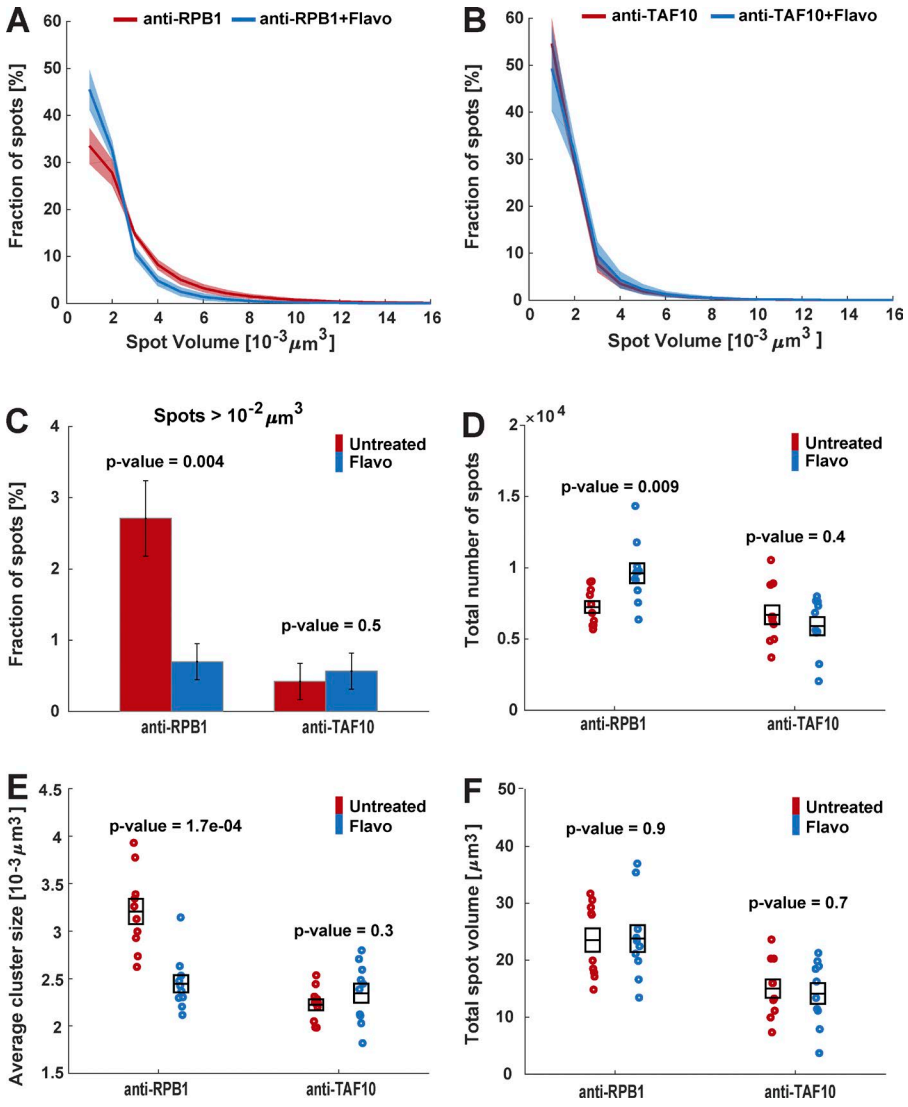

Figure 5. **Quantification of transcription factor distribution in single cells by using VANIMA and super-resolution microscopy. (A)** U2OS cells were transduced with Alexa Fluor 488–labeled anti-RPB1 mAb and then treated with Flavo (2 µM) for 1 h or not (Untreated). 24 h after treatment the cells were fixed and analyzed by 3D-SIM. The number of individual spots and their volume in individual nuclei were quantified by using Fiji/ImageJ and Matlab software. The graph shows the percentage of spots with a given volume in untreated (red) and treated cells with Flavo (blue) acquired from 10 individual cells for each condition. **(B)** Same treatment and analysis as in A, but an Alexa Fluor 488–labeled anti-TAF10 antibody was transduced. **(C)** Spot volumes were extracted from A and B, and the percentage of spots of RPB1 and TAF10 with a volume >10^{-2} µm^3 in the untreated (red) and Flavo (blue) treated cells is shown. The error bars represent the SE from 10 individual cells for each condition. **(D)** Total number of RPB1 and TAF10 spots in 10 individual nuclei for each condition are represented. **(E)** Mean cluster size of the RPB1 or TAF10 spots in 10 individual cells for each condition is shown. **(F)** Total spot volume of RPB1 and TAF10 in 10 individual nuclei for each condition is represented. All black boxes in D–F represent the means and their SEs for each sample. All p-values were calculated by using the two-sample *t* test.

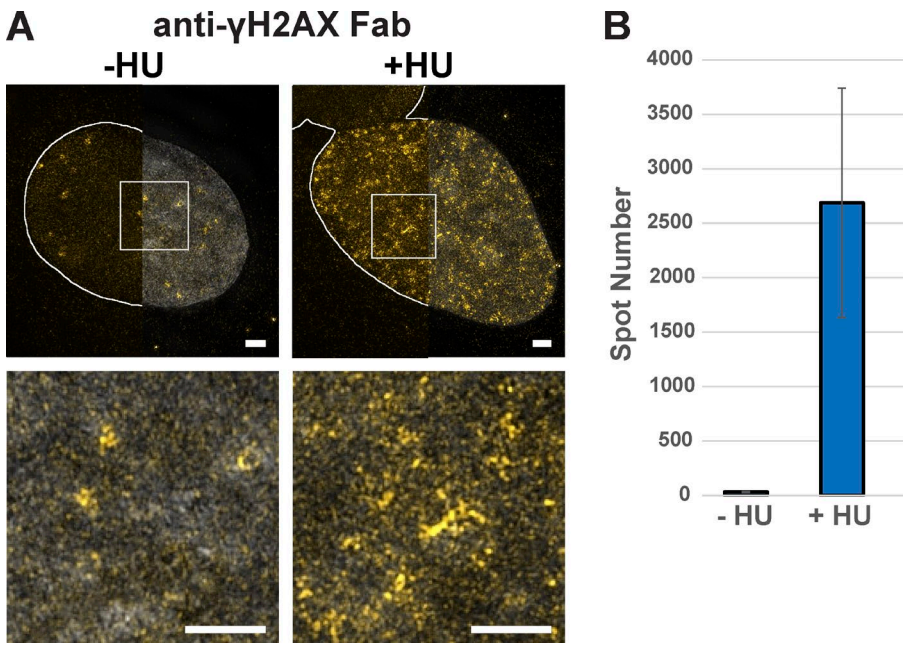

Figure 6. **Imaging of phosphorylated H2AX with VANIMA by super-resolution microscopy. (A)** The labeled anti-γH2AX Fab (yellow) was transduced in U2OS cells, and its localization in the nucleus was recorded by 3D-SIM after treatment with HU for 48 h (+HU) and staining with DAPI (gray). Untreated cells (–HU) were used as the control. The Z maximum intensity projections of 20 slices show the labeled anti-γH2AX Fab with (right half) or without (left half) DAPI counterstaining (gray). The solid white lines depict the nuclear contour. Bottom panels: magnification of the white regions of interest, under the corresponding image (Videos 5 and 6). Bars, 2 µm. **(B)** The number of spots presented in the nuclei as shown in A after quantification with Fiji/ImageJ software. Error bars represent the SD obtained with five recorded cells for each condition.

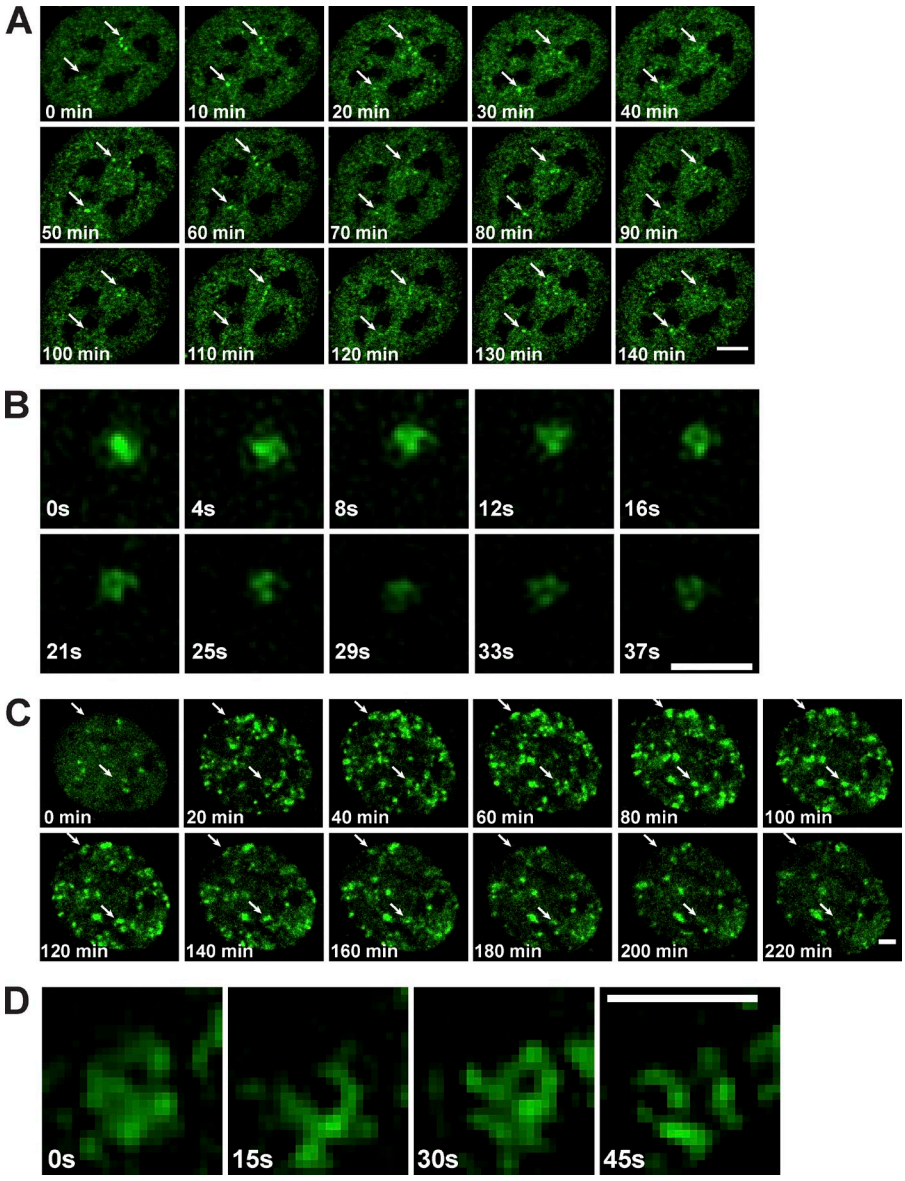

Figure 7. **Live imaging of transcription factors by using VANIMA. (A)** 24 h after electroporation, U2OS cells transduced with Alexa Fluor 488–labeled anti-RPB1 mAb were subjected to live-cell analysis by confocal microscopy focusing on one z section of individual nuclei. They were imaged over a period of 2.5 h and pictures taken every 10 min (Video 7). Arrows point to two larger Pol II cluster examples that move over time. Bar, 5 µm. **(B)** Imaging by 3D-SIM microscopy of an individual Pol II cluster observed in U2OS after transduction as in A. The images were taken over a period of 37 s every 4.1 s and show a maximum intensity projection of the 3D video (Video 8). Bar, 1 µm. **(C)** U2OS cells transduced as in A with the labeled anti-γH2AX Fab were subjected to live-cell analysis by spinning-disk confocal microscopy after the addition of NCS to the culture medium. Pictures were taken every 10 min over a period of 4 h (Video 9) and by focusing on a single z plane. The first time point (0 min) corresponds to the time of the drug addition. Arrows point to γH2AX clusters that appear and disappear over time. Bar, 5 µm. **(D)** Imaging of an individual γH2AX cluster by 3D-SIM microscopy observed in U2OS cells after transduction as in C. Images were recorded over a period of 45 s every 15 s (Video 10). The first time point (0 s) shown was taken 10 min after NCS treatment. Bar, 0.8 µm.

periments (Fig. 3 A), these observations suggest that the labeled mAb does not interfere with the transcription process.

Next, we visualized the induction of γH2AX-Fab labeled foci after NCS treatment by both confocal spinning disc microscopy (Fig. 7 C and Video 9) and 3D-SIM (Fig. 7 D and Video 10). These live-cell experiments demonstrate that the NCS-induced γH2AX foci form large clusters in a kinetic manner and that some of these clusters are stable in time, whereas others are increasing in size, suggesting that the Fab does not hinder the phosphorylation process. Thus, our antibody approach used for live imaging uncovered novel dynamic behaviors of transcription factors and PTM events of H2AX in real time.

Discussion

VANIMA is "right and fair"

Tens of thousands of full-length antibodies that specifically recognize targets with high affinity have been developed over the past decades and are available, mostly commercially. as research tools. Antibodies normally cannot cross intact cellular or subcellular membranes in living cells because of their large size and hydrophilicity (Marschall et al., 2011, 2014). Here we show that electroporation of labeled primary antibodies into live cells allows their efficient delivery into the cytoplasm of cells without significantly reducing their viability. Because full-length mAbs raised against nuclear proteins cannot enter the nucleus, the labeling observed in the nucleus over time can only be explained by the binding of the mAbs to their neosynthesized target and the subsequent import of the labeled mAb-antigen complex to the nucleus. Thus, VANIMA can be used for the characterization of cytoplasmic/nuclear turnover rates of newly synthetized nuclear proteins in live cells when using full-length mAbs. Moreover, the electroporation procedure allows the amount of delivered mAb or Fab to be tightly controlled for the specific and equimolar detection of target proteins (Fig. 1 B; Van Regenmortel, 2014) and hence can also be used for determining the abundance of the accessible antigens in the cell. It is important to note, however, that antibodies have to be charac-

terized for their noninterfering nature before they can be used for tracking native proteins or PTMs. It is likely that VANIMA can also be used with in vitro identified blocking antibodies to disrupt nuclear protein function in living cells.

The use of plasmid cDNA-based transfection assays to exogenously express FTPs is relatively rapid but suffers from the cell-to-cell variability and often protein overexpression (Fig. S2 B). This can be overcome by the generation of stable cell lines, expressing FP-tagged proteins to low levels, which could often take several months. To avoid exogenous protein expression, the genetic knock-in of FP tags into endogenous loci of cells with the use of the CRISPR/Cas9 technology can be used, but the characterization and genotyping of the knock-in could be labor intensive and time consuming because of relatively low efficiency. In addition, in the case of multicolor imaging, changing the colors of the knocked-in tags becomes again very time consuming, when compared with changing the dyes before conjugating them to the purified antibodies. In addition, nanobodies (VHH) derived from camelids, became popular recently for imaging because of their small size (15 kD). However, the generation of these recombinant cDNA expression tools, including their validation for imaging purposes, can be time consuming (Rothbauer et al., 2006; Rinaldi et al., 2013; Krah et al., 2016). Thus, our approach based on already available noninterfering antibodies is much faster and more reliable than any until now described antibody- or antibody fragment-delivery–based visualization method, while giving information on the behavior of endogenous targets.

VANIMA toward uncovering single-cell dynamic behaviors of transcription factors and PTM events in real time

The application of VANIMA to endogenous transcription factors and to a PTM of histone H2AX allowed the precise tracking of these targets in the 3D nucleus and in real-time. Thus, by using VANIMA, dynamic processes of fundamental biological mechanisms, also involving PTMs, can be visualized in nonfixed cells at high resolution. Our results suggest that the detected larger Pol II foci may contain several transcribing Pol II assemblies or Pol II "trains" (Tantale et al., 2016) possibly organized in topological associated domains and/or other control regions (Cisse et al., 2013; Zhao et al., 2014; Cho et al., 2016; Hnisz et al., 2017). The fact that the VANIMA-detected native Pol II foci became smaller when inhibiting transcription with a drug that inhibits transcription elongation is in agreement with previous studies that demonstrated by photobleaching techniques in the whole nuclear compartment that Pol II leaves the chromatin and becomes more mobile (Kimura et al., 2002; Hieda et al., 2005; Vosnakis et al., 2017). It is thus conceivable that the smaller spot size that we observed after Flavo treatment corresponds to "free" Pol II molecules. Note that previous studies visualizing exogenously expressed tagged RPB1 (α-amanitin resistant or not) after shorter Flavo treatment with different super-resolution techniques did not observe significant changes in Pol II spot size (Cisse et al., 2013; Zhao et al., 2014; Cho et al., 2016). Thus, it seems that VANIMA, through detecting endogenous factors, has an improved sensitivity when compared with previously reported RPB1-tagging–based imaging methods. Nevertheless, we also show that large Pol II foci are constantly forming, dynamically associating, and dissociating. By using VANIMA coupled to live 3D-SIM and/or other genome-labeling technologies, it will become possible to investigate, characterize, and dissect the function of the detected endogenous Pol II foci.

In addition, we have been able to monitor with high resolution an essential signal of nuclear DNA damage after insults with genotoxic drugs. In agreement with a recent study, we found that the phospho-H2AX foci correspond to clustered structures (Natale et al., 2017). Moreover, we show here for the first time that these clusters are spatially reorganized with time, likely because of the remodeling of the chromatin, which is necessary for the access of DNA repair proteins. The fact that some clusters come out of focus with time during the analysis is proof of the dynamic aspect of this histone modification. Because analyses with VANIMA are not restricted to endpoint experiments, it might be possible now to further highlight the precise cross talk between transcription and DNA repair. This will likely allow researchers to dissect how an injured cell manages the balance between death and survival.

Moreover, VANIMA coupled with 3D-SIM is suitable for high-resolution colocalization analyses by using up to four different colors. It may allow the in vivo colocalization of several factors within transcription complexes (such as Pol II and TBP in preinitiation complexes) and/or the colocalization of a defined transcription factor with visualizable genomic loci in live cells. These live colocalization studies would help elucidate dynamic nuclear processes based on the association and dissociation of regulatory factors with distinct labeled genomic locations or topological associated domains.

In conclusion, we have developed a strategy that is simple to implement for visualizing target antigens in their native form without fixation that can affect cell integrity (Schnell et al., 2012) and without causing any toxicity in the treated cells. Labeling of endogenous nuclear proteins with VANIMA strictly corresponds to the true antibody–antigen complexes that are taking place in the cell after antibody delivery. We believe that this approach can be used for live- and single-cell super-resolution detection of a large variety of factors and PTMs. Moreover, our method showing that labeled antibodies can be easily and efficiently delivered to cells, overcomes the previously frustrating antibody-delivery limitation issues in biomedicine. Thus, the cellular delivery of antibodies described in our study may also provide extremely useful tools against the fight of a variety of diseases.

Materials and methods

Cell culture

The human U2OS osteosarcoma cells (HTB-96; American Type Culture Collection [ATCC]) were maintained in DMEM supplemented with 10% FCS and 40 µg/ml gentamicin. Human foreskin fibroblast cells (SCRC-1041; ATCC) were cultivated in DMEM/F12 with GlutaMAX-I supplemented with 10% FCS, 15 mM Hepes, 100 UI/ml penicillin, and 100 µg/ml streptomycin. Mouse embryonic stem cells were maintained in DMEM supplemented with 15% FBS (Millipore), 100 UI/ml penicillin, 100 µg/ml streptomycin, 2 mM L-glutamine, 0.1 mM nonessential amino acids, 0.1% β-mercaptoethanol, 1,500 U/ml leukemia inhibitory factor and 2i inhibitors (Ying et al., 2008), 3 µM CHIR99021, and 1 µM PD0325901 (Axon Medchem) on plates coated with 0.1% gelatin solution in 1× PBS (PAN BIO TECH). All these cell lines were maintained in a 5% CO_2 atmosphere at 37°C. Schneider S2 cells (CRL-1963; ATCC) were cultivated by using SCHNEIDER medium containing 10% FCS (heat inactivated)

and 0.5% penicillin/streptomycin and were grown at 27°C. After electroporation the cells were cultivated for 24 h in their corresponding medium without any antibiotics.

Plasmids and transfection procedure

Four mammalian constructs were used for ectopic expression of fluorescent fusion proteins. The expression vectors for HA-GFP, GFP-hRPB1, CFP-hTAF10, and GFP-hTBP were described previously (Soutoglou et al., 2005; de Graaf et al., 2010; Vosnakis et al., 2017). The Flag-Venus microhomology-mediated end-joining (MMEJ) template (hTAF10-MMEJ) and the plasmid expressing three guide RNAs (one targeting the exon 1 of hTAF10 and two targeting the MMEJ template) and coexpressing Cas9-mCherry (hTAF10-Cas9) were assembled by Megawhop (Miyazaki, 2011) and golden gate cloning (Engler et al., 2009), respectively. For transfection, cells were plated into 12-well plates containing 18-mm-high precision cover glasses (Marienfeld) 1 d before transfection to achieve a confluency of ∼70–80%. They were transfected with 100 ng of the corresponding plasmid (GFP-hRPB1, CFP-hTAF10, GFP-hTBP, or HA-GFP) by using Lipofectamine 2000 reagent (Thermo Fisher) following the manufacturer's instructions. The cells were fixed 48 h after transfection for confocal imaging by using the protocol described in the section Sample preparation for imaging.

Antibodies and Fab fragments

The mouse mAbs against RPB1 (1PB-7G5 mAb), TAF10 (6TA-2B11 mAb), TBP (3TF1-3G3 mAb), and bacterial MBP (17TF2-1H4 mAb) were described previously (Lescure et al., 1994; Bertolotti et al., 1996; Zeder-Lutz et al., 1999; Lebedeva et al., 2005; Helmlinger et al., 2006). The anti–α-tubulin antibody was purchased from Sigma-Aldrich (clone DM1A). The anti-γH2AX antibody (14HH2-1H2 mAb) was generated by immunizing mice with the phosphorylated peptide (KATQA[phosphoS]QEY) as described previously (Muratoglu et al., 2003). Specificity of the new antibody was tested by ELISA (Fig. S1 E). Antibodies were purified by using preequilibrated Protein G Sepharose Fast Flow (GE Healthcare) in a batch purification for 2 h at 4°C. Afterward the Sepharose beads were transferred to a Poly-Prep Chromatography column (Bio-Rad) and washed for 20 column volumes with 1× PBS to remove any unspecific bound proteins. The antibodies were eluted in 1-ml fractions by using 0.1 M glycine, pH 2.7, and were directly neutralized with 70 µl of 1 M Tris-HCl, pH 8.2. The fractions containing most of the antibodies were pooled and dialyzed against 1× PBS before 10% glycerol was added to store the aliquoted antibodies at −80°C. Fab fragments of our mAbs were prepared by using the Pierce Mouse IgG1 Fab and $F(ab')_2$ Preparation kit (Thermo Fisher). Preparation was performed as written in the manufacturer's protocol by using a total amount of 1 mg mAbs and digesting them with ficin for 5 h at 37°C. Alternatively, the Fab fragments were prepared by digestion with papain (Sigma-Aldrich). The antibodies were cleaved into Fab fragments by addition of 400 ng papain per milligram of antibody. After incubation for 3 h at 37°C, the Fab fragments were separated from the Fc fragments and undigested antibody molecules by protein A Sepharose chromatography. Unbound Fab fragments were subsequently purified by size exclusion chromatography on a Superdex 75 10/300 (GE Healthcare) equilibrated in PBS. The recovered Fab were stored at 4°C at a concentration of 5 mg/ml.

Antibody labeling

All mAbs and Fab fragments were fluorescently labeled by using the same protocol. A solution containing 100 µg of antibodies or Fab fragments was dialyzed against 0.1 M sodium bicarbonate (Sigma-Aldrich) for 4 h at 4°C using DiaEasy dialyzing tubes (BioVision) to increase labeling efficiency by raising the pH of the antibody solution over a pH of 8. The labeling reaction was performed following the protocol of the Alexa Fluor Monoclonal Antibody Labeling kit (Thermo Fisher) to label 100 µg antibody or Fab fragment randomly with for example Alexa Fluor 488 dyes (A20181). Labeling efficiency was calculated by using the formula given in the manufacturer's protocol. The Alexa Fluor 488 dyes have a tetra-fluoro-phenyl ester moiety, which reacts with primary amines of proteins to form a covalent dye–protein conjugate. This labeling strategy results in a high labeling density with up to five to seven dyes per molecule of antibody.

Note of caution: To label antibodies or Fabs, we have used *N*-hydroxysuccinimide ester fluorophores that react with the amine group at the tip of the side chain of lysines. This is a conventional method of chemical labeling of proteins, which works fine with antibodies that do not harbor lysine residues in their binding site (paratope). If the quality of binding of the labeled Fab (that can be easily tested by IF) is affected by this technique and when the antibody is precious, we propose to set up a site-directed labeling, which consists in the preparation of $(Fab')_2$ fragments, which can be specifically labeled at the typical cysteine residues in the C-terminal of the Fab' (hinge region) with maleimide-activated fluorophores upon mild reduction. The scaffold cysteines present in the different IgG fold-domains of the Fab' are not accessible under these conditions. This method allows the addition of a maximum of two to three fluorophore molecules per Fab and preserves the antibody-binding site from any deleterious chemical alteration.

Electroporation procedure

Transductions were performed by using the Neon Transfection system (MPK5000; Thermo Fisher) and the corresponding Neon kits (MPK1096 or MPK10096; Thermo Fisher). To transduce 10^5 cells, the 10-µl Neon tips were used with 0.5–4 µg antibodies or Fab fragments; however, to transduce 1.2 x10^6 cells with 6–48 µg antibodies, the 100-µl Neon tips were used. The desired number of cells (depending on the number of transductions performed) were trypsinized and washed once with 4 ml 1× PBS before the pellet was resuspended in the supplied resuspension buffer. The volume corresponding to 1×10^5 or 1.2×10^6 cells was mixed with the labeled antibody or Fab solution and immediately transduced by using the following parameters: 1550 V, 3 pulses, and 10 ms per pulse. After transduction, the cells were transferred directly into 12-well plates (Corning) containing prewarmed medium without antibiotics. The medium was changed to antibiotic containing medium 24 h after transduction if the cells were used for live imaging; otherwise, they were fixed directly for fixed-cell imaging. Transduction efficiency was tested 24 h after electroporation of anti-RPB1 (1PB-7G5) mAb by counting 100 cells by using a confocal microscope to determine the percentage of cells showing a fluorescent signal in the nucleus. Cell viability after electric shock was determined by measuring the percentage of living cells before and after transduction by using a Countess II Cell Counter (Thermo Fisher) and Trypan blue staining of dead cells and normalization to the cell viability before electroporation.

Note of caution: The cells should not stay >20 min in the resuspension buffer, because the cell viability will decrease drastically. If many transductions need be performed, it can be advantageous to prepare several cell pellets and resuspend them one by one.

In the past, we tried classical electroporation with cuvettes to deliver antibodies inside cells, but this approach was not so successful, because the majority of the treated cells were dying after the electric shock (one pulse). The Neon apparatus used in this study corresponds to a novel electroporation device with a capillarity electrode. The design of the electrode in pipette (and not in cuvette) has been shown to produce a more uniform electric field within a small volume, which results in less toxicity to the cells without loss of transfection efficiency.

This apparatus is commercially available for DNA or siRNA transfection. However, we adapted the setting of several parameters (voltage, number of pulses, and efficiency of internalization) for optimal protein delivery. To our knowledge, this achievement allows nearly all treated cells to be transduced without loss of viability. Importantly, the same Neon electroporation apparatus has also been used successfully to deliver proteins in cells (Clift et al., 2017).

Sample preparation for imaging

For fixed sample preparation, the transduced cells were transferred to 12-well plates containing 18-mm-high precision cover glasses (Marienfeld). They were fixed 24 h after electroporation by using 4% PFA (Electron Microscopy Sciences) in 1× PBS prewarmed to 37°C for 5 min. Afterward the cells were washed twice for 5 min at RT with 1× PBS plus 0.02% Triton X-100, once with 1× PBS, once with 1× PBS plus 0.1% Triton X-100 for 20 min at RT, and then again twice for 5 min at RT with 1× PBS plus 0.02% Triton X-100 and once with 1× PBS. Next, the cells were incubated with a DAPI solution in dH_2O (1/2,500 dilution from 1 mg/ml stock solution; Sigma-Aldrich) for 30 s and afterward mounted with Vectashield (H1000, not containing DAPI; Vector Laboratories) if the samples were used for 3D-SIM microscopy. When samples were prepared for visualization with the use of confocal microscopy, they were directly mounted with Vectashield mounting medium containing DAPI (H1200; Vector Laboratories).

Because the target is already labeled with the transduced antibody, most of the washing steps mentioned in the section above are optional and are needed only if the signal-to-noise ratio during imaging is too low because of nontransduced antibodies, which can stick on the coverslip surface.

For classical IF, the cells were seeded as described before, but the day before the experiment to achieve a confluency of ∼70–80%. The fixation protocol was the same as for the transduced samples except that all wash steps are mandatory and there are additional incubation steps with the primary and secondary antibodies. After fixation as described above, the cells were permeabilized by using 1× PBS plus 0.1% Triton X-100 for 20 min at RT and then incubated with 2 µg primary antibody (anti-RPB1, anti-TAF10, or anti-TBP) diluted in 1× PBS plus 10% FCS for 1 h at RT. The negative control was incubated only with buffer missing any primary antibody. The cells were washed three times for 5 min at RT twice with 1× PBS plus 0.02% Triton X-100 and once with 1× PBS followed by an incubation with the Alexa Fluor 488–conjugated anti-mouse secondary antibody (Thermo Fisher) diluted 1/3,000 in 1× PBS plus 10% FCS for 1 h at RT. After three more washings for 5 min at RT, samples were mounted using Vectashield containing DAPI for confocal imaging. To eliminate all soluble proteins before fixation and to visualize chromatin-bound RPB1, the cells were treated with CSK buffer (100 mM NaCl, 3 mM $MgCl_2$, 10 mM Hepes, 300 mM sucrose, 0.3% Triton X-100, and protease inhibitor cocktail) before fixing with PFA for 10 min at RT.

For live-imaging the cells were transferred to µ-dishes (35-mm-diameter, high, glass bottom; ibidi) for confocal imaging or to µ-slides (8-well, glass bottom; ibidi) for 3D-SIM imaging after transduction containing prewarmed medium and incubated at 5% CO_2 and 37°C until imaging started. Before imaging the medium was changed to the described growth medium without phenol red for confocal imaging or Leibovitz's L-15 medium (Thermo Fisher) for 3D-SIM microscopy.

Transcription inhibition

Inhibition of transcription was achieved by treating U2OS cells either with α-amanitin (Molekula) or Flavo (Flavo hydrochloride hydrate; Sigma-Aldrich). Electroporated cells were incubated 6 h after transduction with 4 µg/ml α-amanitin overnight. Flavo treatment was performed 24 h after transduction by incubating the cells with 2 µM Flavo for 1 h.

DNA damage induction

For γH2AX imaging, DNA damage in the form of double-strand breaks was induced by using either HU (Sigma) or NCS (Sigma). For HU treatment, the cells were transduced with 2 µg anti-γH2AX Fab antibody and 12 h later treated with 2 mM HU for 48 h before the cells were fixed. To induce DNA damage with NCS, the cells were transduced as described before and 22 h later incubated with 100 ng/ml NCS for 15 min. Afterward the medium was changed to classical growth medium, and the cells were incubated for 2 h more before fixation. For γH2AX live imaging, the same protocol was followed except that 50 ng/ml (confocal microscopy) or 200 ng/ml (3D-SIM microscopy) NCS was added immediately before image acquisition.

Confocal microscopy

Confocal imaging of fixed samples was performed on an SP8UV microscope (Leica) equipped with a 561-nm DPSS laser, a 633-nm HeNe laser, a 405-nm laser diode, and a 488-nm argon laser. A 63× oil immersion objective (NA 1.4) was used, and images were taken by using the hybrid detector photon-counting mode. Confocal live imaging was performed on either an SP8X microscope (Leica) equipped with a white light laser (Leica) by using the 488-nm laser line or a Ti microscope (Nikon) equipped with a CSU-X1 confocal scanner (Yokogawa) and an Evolve back-illuminated EMCCD camera (Photometrics). 2D videos from the SP8X microscope were taken using a 63× oil immersion objective (NA 1.4) on photomultiplier tube detection mode and time intervals of 10 min. The Ti microscope 2D videos were taken using a 60× oil immersion objective (NA 1.4), an exposure time of 800 ms, and time intervals of 10 min. All images and videos were subsequently analyzed and processed by using Fiji/ImageJ software.

3D-SIM super-resolution microscopy and image analysis

3D-SIM was performed on a DeltaVision OMX-Blaze V4 system (GE Healthcare) equipped with a Plan Apo N 60× (1.42 NA) oil immersion objective lens (Olympus), four liquid-cooled sCMOS cameras (pco. edge 5.5, full frame 2,560 × 2,160; PCO) and 405-, 445-, 488-, 514-, 568-, and 642-nm solid-state lasers. The 405-, 488-, and 568-nm laser lines were used during acquisition, and the optical z sections were separated by 0.125 µm. For fixed cells, laser power was attenuated to 10 or 31.3%, and exposure times were typically between 75 and 400 ms. Live imaging of RPB1 or γH2AX was performed by using a laser power attenuated to 10 or 31.3% and an exposure time of 10–25 ms with time intervals of either 4.1 or 15 s and a total acquisition time of 45 s. The raw images were processed and reconstructed by using the DeltaVision OMX SoftWoRx software package (v6.1.3; Applied Precision).

For the 3D-SIM images in Fig. 4 and Fig. 6 A, the outline for the nucleus (DAPI channel) was defined after applying in Fiji a Gaussian blur (σradius 4), applying a threshold to match the nucleus outline ("mean algorithm"), and the outline was detected by using the "Analyze Particle" (with option "Include Holes"). The resulting outline was shown on the channel of interest, and the look-up table "Yellow Hot" has been applied to the image for a better visualization. The SIMcheck Fiji/ImageJ plugin (Ball et al., 2015) was used to check raw and reconstructed image quality. Channel intensity profiles, Fourier plots, motion and illumination variation, as well as modulation contrast to noise maps have been tested for all 3D-SIM images and are in general above the required thresholds.

The image processing and quantification was performed by using the Imaris software (Bitplane) for preparing 3D videos or Fiji/ImageJ software and in particular the 3D spot segmentation (Ollion

et al., 2013) as well as the 3D object counter (Bolte and Cordelières, 2006) for the quantification of the 3D images. In brief, the spots were segmented by finding local maxima in the image and afterward fitting a Gaussian distribution locally. As soon as the mask of each spot was available, factors such as spot number or volume could be computed. Finally, analysis of the spot data was performed by using Matlab (MathWorks). Distributions of spot volumes with the use of antibodies against RPB1 or TAF10 were computed by averaging the histograms of measured spot volumes >10 cells for each condition (Flavo-treated vs. untreated). In addition, the mean fraction of spots bigger than 10^{-2} μm^3 in each condition was reported. P-values were calculated by using the two-sample *t* test that allows to determine whether two population means are significantly different.

Flag-Venus hTAF10 knock-in

The knock-in of the Flag-Venus coding sequence at exon 1 of the hTAF10 gene was performed by using CRISPR/Cas9 and MMEJ (Nakade et al., 2014). In brief, U2OS cells were cotransfected with the hTAF10-Cas9 and hTAF10-MMEJ plasmids at a ratio of 2:1 by using FuGENE HD (Promega). After 48 h, cells that had taken up the Cas9 plasmid (mCherry positive) were sorted by flow cytometry (FACS ARIA; BD Biosciences) and cultured under limiting dilution conditions. Colonies were expanded and genotyped by PCR and tested for Flag-Venus tag insertion by IF. Sequencing of the PCR products confirmed the in-frame insertion of the Flag-Venus sequence. Note that all the three knock-in clones obtained were heterozygous.

Immunoprecipitation

For electroporation-immunoprecipitation (Elec-IP), 1.2×10^6 cells were transduced with 6–48 µg anti-RPB1 7G5 (corresponding to 0.5–4 µg antibody in 1×10^5 cells) 24 h before protein extraction. Cells treated with the same electric shock, but without any antibody, were used as a mock control. The cells were trypsinized and whole-cell protein extracts were produced by solubilizing the cell pellets in 40 µl RIPA buffer (50 mM Tris-HCl, pH 7.6, 150 mM NaCl, 1% NP-40, 1% sodium deoxycholate, and 0.1% SDS) and incubating them for 5 min on ice. The concentration of the extracts was determined by using a standard Bradford assay, and 30 µg extract was mixed with 100 µl of equilibrated protein G–coupled magnetic Dynabeads (Thermo Fisher) for an immunoprecipitation overnight at 4°C. Next, the Dynabeads were separated from the supernatant containing nonbound proteins and were washed three times with IP500 buffer (25 mM Tris-HCl, pH 7.9, 0.1% NP-40, 5 mM $MgCl_2$, 10% glycerol, 500 mM KCl, 2 mM DTT, and protease inhibitor cocktail) and two times with IP100 buffer (25 mM Tris-HCl, pH 7.9, 0.1% NP-40, 5 mM $MgCl_2$, 10% glycerol, 100 mM KCl, 2 mM DTT, and protease inhibitor cocktail) to remove any unspecific bound proteins. The beads with the bound antibody-protein complexes were stored in IP100 buffer. The input protein extracts, the supernatant of the Elec-IP, as well as the beads were analyzed afterward by Western blot.

Western blot analysis

Whole-cell protein extracts were prepared from cells washed twice with 1× PBS by using RIPA buffer (see the previous section). Elec-IP fractions were loaded on 4–15% precast SDS-PAGE gels (Bio-Rad) with Laemmli buffer. Protein transfer on nitrocellulose membranes was performed by using Mini Protean II tanks (Bio-Rad). Western blots were blocked by using 3–5% milk for at least 30 min before overnight incubation with the primary antibody against RPB1 (1PB-7G5 mAb, 1:1,000). Signal was detected by incubating for 1 h with HRP-conjugated secondary antibodies (1:10,000; Jackson ImmunoResearch) and revealed by using ECL (Thermo Fisher) and ChemiDoc Touch Imaging System (Bio-Rad).

Pre-mRNA transcription analysis

24 h before total RNA extraction, 1.2×10^6 U2OS cells were transduced with 24 µg anti-RPB1, anti-TBP, or anti-TAF10 antibodies. U2OS cells electroporated but without transduction of antibody were used as controls. Additionally, electroporated U2OS cells without transduction of antibody were treated with 4 µg/ml α-amanitin overnight as a positive control for transcriptional inhibition. As negative control, 24 µg an antibody targeting the bacterial MBP was transduced into U2OS cells. Total RNA was extracted by using Tri Reagent (Molecular Research Center, Inc.) and following manufacturer's instructions. Removal of genomic DNA contamination was achieved by using the TURBO DNA-*free* kit (Thermo Fisher). For reverse transcription, 3.2 µg of random hexamer primers (Thermo Fisher), dNTP Mix (Thermo Fisher), and Transcriptor Reverse transcription (Roche) were used following manufacturer's instruction. For qPCR, the cDNA samples were diluted and amplified by using SYBR Green 2× PCR Master Mix I (Roche) and a LightCycler 480 Instrument II (Roche) with the following program: one cycle of 5 min at 95°C for predenaturation, 45 amplification cycles with 10 s at 95°C for denaturation, 20 s at 65°C for primer annealing, and 20 s at 72°C for extension. Melting curves were determined between 65°C and 97°C followed by one cycle of cooling for 30 s at 40°C. Primer pairs used for qPCR are listed in Table S2. To quantify newly synthesized RNA Pol II transcripts, primer pairs amplifying from an intron to an exon were designed, therefore reflecting unspliced transcripts. The genes analyzed were selected randomly and represent genes of different chromosomes. However, because unspliced transcripts are a minority in total RNA extracts, the genes selected are mostly highly expressed genes. The obtained threshold-values were used to calculate the relative fold change by using the $\Delta\Delta C_T$ method by normalization to RNA Pol III transcripts (*RPPH1* and *RN7SK*) and taking into account primer efficiencies. The heatmap was based on the mean fold change, with the U2OS cells electroporated but without transduction sample set to zero change in expression and was generated by using R 3.4.3 and RStudio 1.1.383 and the ComplexHeatmap (Bioconductor) package.

Cell cycle analysis

For cell cycle analysis, 1.2×10^6 U2OS cells were electroporated with 24 µg anti-RPB1, anti-TAF10, or anti-TBP antibody. As controls, electroporated cells without any antibody were used. As positive control for transcriptional inhibition, electroporated cells without any antibody were treated with 4 µg/ml α-amanitin overnight. As negative control, 24 µg anti-MBP was transduced into U2OS cells. The cells were harvested 24 or 48 h after electroporation, washed with 1× PBS, and fixed in 70% ethanol. Fixed cells were stained with 15 µg/ml propidium iodide (Sigma-Aldrich) and treated with 75 µg/ml RNase A (Thermo Fisher) for 1 h before the FACS analysis. FACS analysis was conducted on a FACS Celesta (BD Biosciences) counting 10,000 cells per sample, and data analysis was performed by using FlowJo 10.2. The cell cycle phases were assigned manually.

Proliferation assay

Proliferation of U2OS cells after antibody transduction was tested by using the Click-it Plus EdU Flow Cytometry Assay kit (C10632; Thermo Fisher). A total amount of 1.2×10^6 cells was transduced with 24 µg anti-RPB1, anti-TAF10, anti-TBP, or anti-MBP antibody and incubated for 24 h at 5% CO_2 and 37°C. As controls transduced cells without any antibody were added either as positive control for normal proliferation or as negative control by adding 4 µg/ml α-amanitin (Molekula) overnight 6 h after transduction to see how proliferation was affected if transcription was inhibited. The cells were treated 24 h after transduction with 10 µM EdU for 1 h to test the proliferation capacity of the cells. Non-EdU treated cells for

every transduction were added as controls. The Click-it reaction with Alexa Fluor 488 was performed as described in the manufacturer's protocol. FACS analysis was performed on a FACS Celesta (BD Biosciences) counting 30,000 cells per sample. The positive control was used for normalization.

Apoptosis assay

To test if the cells would undergo apoptosis after transduction of antibodies, an APOPercentage apoptosis assay (Biocolor) was performed. U2OS cells (1×10^5) were transduced with 2 µg anti-RPB1, anti-TAF10, anti-TBP, or anti-MBP antibody and incubated for 24 h at 5% CO_2 and 37°C. As negative (0% apoptosis) control, electroporated cells without antibodies were used. As positive (100% apoptosis) control, cells were treated 20 h after transduction, without antibodies, with 10 mM H_2O_2, for 4 h to induce apoptosis. The apoptosis assay was performed as described in the manufacturer's protocol for the colorimetric assay. The results were normalized to the positive control.

Suitability of new antibodies for VANIMA

According to our experience, antibodies that recognize their epitopes in the intracellular context are the ones that have a good chance of working in VANIMA. We have observed that those antibodies that work fine when tested by IF also work in our live-cell imaging assays. This shows that the accessibility of the epitope in the intracellular context is the limiting factor and that likely all antibodies that are used for imaging in fixed cells will be excellent candidates for the VANIMA application. Within a set of 25 different antibodies that were all working in IF, only one was not adequate for VANIMA. In this case, we found that the epitope was hidden after neosynthesis in the cytoplasm and it became accessible only when the antigen was imported in the nucleus (Freund et al., 2013). After an assessment of the quality of the antibody in IF, it should be purified and labeled with fluorescent dyes as described in the Antibody labeling section. Depending on the localization of the target protein (nucleus or cytoplasm), a digestion of the antibody to Fab fragments could be considered. To identify the amount of antibody or Fab that needs to be electroporated to bind a suitable amount of target protein, a titration electroporation similar to the one shown in Fig. 1 B should be performed. It is important to note that amounts >10 µg antibodies or Fabs should be avoided because at this point the amount of protein electroporated starts to get toxic for the cells. Afterward, the binding of the antibody to the intracellular target should be verified by immunoprecipitation after electroporation as shown in Fig. 1 C or by performing an IF-electroporation comparison as shown in Fig. 2 C (and Fig. S1 C) depending on if the desired antibody has several or only one epitope on the target protein. The last step would be to verify if the antibody is blocking functions of the target protein or affecting the survival of the cells. A first indication is the viability of the cells after electroporation which should be, depending on the cell line used, >60–90% (see also Table S1). Other validation experiments would be to test the proliferation of the cells and the cell cycle progression or if apoptosis occurs (Fig. 3, B–E). Depending on the target protein, also more specific validation experiments should be considered as the premRNA transcription analysis for transcription factors (Fig. 3 A). After these validation tests, the antibody or Fab can be used for fixed- or live-cell imaging of endogenous proteins.

Online supplemental material

Fig. S1 shows different experiments to verify the efficiency (A), localization (B and D), target binding (E), and affinity (C) of different antibodies using VANIMA. Fig. S2 shows the imaging of transcription factors with classical labeling methods such as IF (A) or the genetic tagging with fluorescent tags (B–E). Table S1 shows electroporation of antibodies is highly efficient, keeping a high viability of the cells, and can be used in many different cell lines. Table S2 shows primers used to quantify RNA Pol II premRNA as well as RNA Pol I and Pol III transcripts. Video 1 shows the transport of labeled anti-RPB1 mAb from the cytoplasm to the nucleus of living cells. Videos 2–4 show nuclei of U2OS cells transduced with either labeled anti-RPB1, anti-TAF10, or anti-TBP mAbs analyzed by 3D-SIM microscopy. Videos 5 and 6 show nuclei transduced with anti-γH2AX Fab and treatment with or without HU analyzed by 3D-SIM microscopy. Video 7 shows confocal live-cell imaging of RNA Pol II using VANIMA. Video 8 shows 3D-SIM live-cell imaging of RNA Pol II clusters. Video 9 shows confocal live-cell imaging of γH2AX foci. Video 10 shows 3D-SIM live-cell imaging of γH2AX foci. Higher-resolution videos of the 3D-SIM videos can be obtained directly from the corresponding authors.

Acknowledgments

We thank T. Sexton, S.D. Vincent, and F. Müller for carefully reading the manuscript and helpful comments; L. Schermelleh for constant support; the Institut de Génétique et de Biologie Moléculaire et Cellulaire (IGBMC) cell culture service for help with the cells; and Y. Lutz, M. Koch, and E. Guiot from the IGBMC imaging platform. L. Tora thanks M. Featherstone for making the starting of this project possible at the School of Biological Sciences, Nanyang Technological University (Singapore).

This work was supported by funds from Conseil National de la Recherche Scientifique, Institut national de la santé et de la rechrche médicale, Université de Strasbourg, Ligue Contre le Cancer (Comité CCIRGE-BFC to E. Weiss), by the European Research Council Advanced Grant (ERC-2013-340551, Birtoaction to L. Tora), and a grant from a French State fund managed by the Agence Nationale de la Recherche (ANR-10-LABX-0030-INRT) under the frame program Investissements d'Avenir (ANR-10-IDEX-0002-02), and core founding from the Agency for Science, Technology, and Research for G.D. Wright.

The authors declare no competing financial interests.

Author contributions: S. Conic and V. Fischer performed experiments. S. Conic, E. Weiss, and L. Tora designed the experiments to develop the protocol. M. Oulad-Abdelghani generated the anti-γH2AX antibody, and D. Desplancq characterized it. K. Babu N. and G.D. Wright performed initial labeling and 3D-SIM experiments. S. Conic and A. Ferrand performed all the 3D-SIM experiments presented in the study. B.R. San Martin and V. Heyer designed and provided vectors for CRISPR/Cas9 knock-in experiments. N. Molina and J. Pontabry carried out image analyses. S. Conic, N. Molina, E. Weiss, and L. Tora wrote the manuscript.

Submitted: 28 September 2017
Revised: 15 December 2017
Accepted: 18 January 2018

References

Ball, G., J. Demmerle, R. Kaufmann, I. Davis, I.M. Dobbie, and L. Schermelleh. 2015. SIMcheck: A toolbox for successful super-resolution structured illumination microscopy. *Sci. Rep.* 5:15915. https://doi.org/10.1038/srep15915

Beghin, A., A. Kechkar, C. Butler, F. Levet, M. Cabillic, O. Rossier, G. Giannone, R. Galland, D. Choquet, and J.B. Sibarita. 2017. Localization-based super-resolution imaging meets high-content screening. *Nat. Methods.* 14:1184–1190. https://doi.org/10.1038/nmeth.4486

Berglund, D.L., and J.R. Starkey. 1989. Isolation of viable tumor cells following introduction of labelled antibody to an intracellular oncogene product

using electroporation. *J. Immunol. Methods.* 125:79–87. https://doi.org/10.1016/0022-1759(89)90080-X

Bertolotti, A., Y. Lutz, D.J. Heard, P. Chambon, and L. Tora. 1996. hTAF(II)68, a novel RNA/ssDNA-binding protein with homology to the pro-oncoproteins TLS/FUS and EWS is associated with both TFIID and RNA polymerase II. *EMBO J.* 15:5022–5031.

Betzig, E., G.H. Patterson, R. Sougrat, O.W. Lindwasser, S. Olenych, J.S. Bonifacino, M.W. Davidson, J. Lippincott-Schwartz, and H.F. Hess. 2006. Imaging intracellular fluorescent proteins at nanometer resolution. *Science.* 313:1642–1645. https://doi.org/10.1126/science.1127344

Bolte, S., and F.P. Cordelières. 2006. A guided tour into subcellular colocalization analysis in light microscopy. *J. Microsc.* 224:213–232. https://doi.org/10.1111/j.1365-2818.2006.01706.x

Boulon, S., B. Pradet-Balade, C. Verheggen, D. Molle, S. Boireau, M. Georgieva, K. Azzag, M.C. Robert, Y. Ahmad, H. Neel, et al. 2010. HSP90 and its R2TP/Prefoldin-like cochaperone are involved in the cytoplasmic assembly of RNA polymerase II. *Mol. Cell.* 39:912–924. https://doi.org/10.1016/j.molcel.2010.08.023

Burgess, A., T. Lorca, and A. Castro. 2012. Quantitative live imaging of endogenous DNA replication in mammalian cells. *PLoS One.* 7:e45726. https://doi.org/10.1371/journal.pone.0045726

Chakrabarti, R., D.E. Wylie, and S.M. Schuster. 1989. Transfer of monoclonal antibodies into mammalian cells by electroporation. *J. Biol. Chem.* 264:15494–15500.

Chao, S.H., K. Fujinaga, J.E. Marion, R. Taube, E.A. Sausville, A.M. Senderowicz, B.M. Peterlin, and D.H. Price. 2000. Flavopiridol inhibits P-TEFb and blocks HIV-1 replication. *J. Biol. Chem.* 275:28345–28348. https://doi.org/10.1074/jbc.C000446200

Cho, W.K., N. Jayanth, S. Mullen, T.H. Tan, Y.J. Jung, and I.I. Cissé. 2016. Super-resolution imaging of fluorescently labeled, endogenous RNA polymerase II in living cells with CRISPR/Cas9-mediated gene editing. *Sci. Rep.* 6:35949. https://doi.org/10.1038/srep35949

Cisse, I.I., I. Izeddin, S.Z. Causse, L. Boudarene, A. Senecal, L. Muresan, C. Dugast-Darzacq, B. Hajj, M. Dahan, and X. Darzacq. 2013. Real-time dynamics of RNA polymerase II clustering in live human cells. *Science.* 341:664–667. https://doi.org/10.1126/science.1239053

Clift, D., W.A. McEwan, L.I. Labzin, V. Konieczny, B. Mogessie, L.C. James, and M. Schuh. 2017. A method for the acute and rapid degradation of endogenous proteins. *Cell.* 171:1692–1706.e18. https://doi.org/10.1016/j.cell.2017.10.033

Courtête, J., A.P. Sibler, G. Zeder-Lutz, D. Dalkara, M. Oulad-Abdelghani, G. Zuber, and E. Weiss. 2007. Suppression of cervical carcinoma cell growth by intracytoplasmic codelivery of anti-oncoprotein E6 antibody and small interfering RNA. *Mol. Cancer Ther.* 6:1728–1735. https://doi.org/10.1158/1535-7163.MCT-06-0808

Cramer, L.P., and T.J. Mitchison. 1995. Myosin is involved in postmitotic cell spreading. *J. Cell Biol.* 131:179–189. https://doi.org/10.1083/jcb.131.1.179

de Graaf, P., F. Mousson, B. Geverts, E. Scheer, L. Tora, A.B. Houtsmuller, and H.T. Timmers. 2010. Chromatin interaction of TATA-binding protein is dynamically regulated in human cells. *J. Cell Sci.* 123:2663–2671. https://doi.org/10.1242/jcs.064097

Desplancq, D., G. Freund, S. Conic, A.P. Sibler, P. Didier, A. Stoessel, M. Oulad-Abdelghani, M. Vigneron, J. Wagner, Y. Mély, et al. 2016. Targeting the replisome with transduced monoclonal antibodies triggers lethal DNA replication stress in cancer cells. *Exp. Cell Res.* 342:145–158. https://doi.org/10.1016/j.yexcr.2016.03.003

Dundr, M., U. Hoffmann-Rohrer, Q. Hu, I. Grummt, L.I. Rothblum, R.D. Phair, and T. Misteli. 2002. A kinetic framework for a mammalian RNA polymerase in vivo. *Science.* 298:1623–1626. https://doi.org/10.1126/science.1076164

Ellenberg, J., J. Lippincott-Schwartz, and J.F. Presley. 1999. Dual-colour imaging with GFP variants. *Trends Cell Biol.* 9:52–56. https://doi.org/10.1016/S0962-8924(98)01420-2

Engler, C., R. Gruetzner, R. Kandzia, and S. Marillonnet. 2009. Golden gate shuffling: a one-pot DNA shuffling method based on type IIs restriction enzymes. *PLoS One.* 4:e5553. https://doi.org/10.1371/journal.pone.0005553

Freund, G., A.P. Sibler, D. Desplancq, M. Oulad-Abdelghani, M. Vigneron, J. Gannon, M.H. Van Regenmortel, and E. Weiss. 2013. Targeting endogenous nuclear antigens by electrotransfer of monoclonal antibodies in living cells. *MAbs.* 5:518–522. https://doi.org/10.4161/mabs.25084

Gorski, S.A., S.K. Snyder, S. John, I. Grummt, and T. Misteli. 2008. Modulation of RNA polymerase assembly dynamics in transcriptional regulation. *Mol. Cell.* 30:486–497. https://doi.org/10.1016/j.molcel.2008.04.021

Hager, G.L., J.G. McNally, and T. Misteli. 2009. Transcription dynamics. *Mol. Cell.* 35:741–753. https://doi.org/10.1016/j.molcel.2009.09.005

Hayashi-Takanaka, Y., K. Yamagata, T. Wakayama, T.J. Stasevich, T. Kainuma, T. Tsurimoto, M. Tachibana, Y. Shinkai, H. Kurumizaka, N. Nozaki, and H. Kimura. 2011. Tracking epigenetic histone modifications in single cells using Fab-based live endogenous modification labeling. *Nucleic Acids Res.* 39:6475–6488. https://doi.org/10.1093/nar/gkr343

Helmlinger, D., S. Hardy, G. Abou-Sleymane, A. Eberlin, A.B. Bowman, A. Gansmüller, S. Picaud, H.Y. Zoghbi, Y. Trottier, L. Tora, and D. Devys. 2006. Glutamine-expanded ataxin-7 alters TFTC/STAGA recruitment and chromatin structure leading to photoreceptor dysfunction. *PLoS Biol.* 4:e67. https://doi.org/10.1371/journal.pbio.0040067

Hernandez, N. 1993. TBP, a universal eukaryotic transcription factor? *Genes Dev.* 7(7b, 7B):1291–1308. https://doi.org/10.1101/gad.7.7b.1291

Hieda, M., H. Winstanley, P. Maini, F.J. Iborra, and P.R. Cook. 2005. Different populations of RNA polymerase II in living mammalian cells. *Chromosome Res.* 13:135–144.

Hnisz, D., K. Shrinivas, R.A. Young, A.K. Chakraborty, and P.A. Sharp. 2017. A phase separation model for transcriptional control. *Cell.* 169:13–23. https://doi.org/10.1016/j.cell.2017.02.007

Kimura, H. 2005. Histone dynamics in living cells revealed by photobleaching. *DNA Repair (Amst.).* 4:939–950. https://doi.org/10.1016/j.dnarep.2005.04.012

Kimura, H., Y. Tao, R.G. Roeder, and P.R. Cook. 1999. Quantitation of RNA polymerase II and its transcription factors in an HeLa cell: Little soluble holoenzyme but significant amounts of polymerases attached to the nuclear substructure. *Mol. Cell. Biol.* 19:5383–5392. https://doi.org/10.1128/MCB.19.8.5383

Kimura, H., K. Sugaya, and P.R. Cook. 2002. The transcription cycle of RNA polymerase II in living cells. *J. Cell Biol.* 159:777–782. https://doi.org/10.1083/jcb.200206019

Krah, S., C. Schröter, S. Zielonka, M. Empting, B. Valldorf, and H. Kolmar. 2016. Single-domain antibodies for biomedical applications. *Immunopharmacol. Immunotoxicol.* 38:21–28. https://doi.org/10.3109/08923973.2015.1102934

Lebedeva, L.A., E.N. Nabirochkina, M.M. Kurshakova, F. Robert, A.N. Krasnov, M.B. Evgen'ev, J.T. Kadonaga, S.G. Georgieva, and L. Tora. 2005. Occupancy of the Drosophila hsp70 promoter by a subset of basal transcription factors diminishes upon transcriptional activation. *Proc. Natl. Acad. Sci. USA.* 102:18087–18092. https://doi.org/10.1073/pnas.0509063102

Lescure, A., Y. Lutz, D. Eberhard, X. Jacq, A. Krol, I. Grummt, I. Davidson, P. Chambon, and L. Tora. 1994. The N-terminal domain of the human TATA-binding protein plays a role in transcription from TATA-containing RNA polymerase II and III promoters. *EMBO J.* 13:1166–1175.

Lukas, J., J. Bartek, and M. Strauss. 1994. Efficient transfer of antibodies into mammalian cells by electroporation. *J. Immunol. Methods.* 170:255–259. https://doi.org/10.1016/0022-1759(94)90400-6

Macháň, R., and T. Wohland. 2014. Recent applications of fluorescence correlation spectroscopy in live systems. *FEBS Lett.* 588:3571–3584. https://doi.org/10.1016/j.febslet.2014.03.056

Manders, E.M., H. Kimura, and P.R. Cook. 1999. Direct imaging of DNA in living cells reveals the dynamics of chromosome formation. *J. Cell Biol.* 144:813–821. https://doi.org/10.1083/jcb.144.5.813

Markaki, Y., M. Gunkel, L. Schermelleh, S. Beichmanis, J. Neumann, M. Heidemann, H. Leonhardt, D. Eick, C. Cremer, and T. Cremer. 2010. Functional nuclear organization of transcription and DNA replication: A topographical marriage between chromatin domains and the interchromatin compartment. *Cold Spring Harb. Symp. Quant. Biol.* 75:475–492. https://doi.org/10.1101/sqb.2010.75.042

Marschall, A.L., A. Frenzel, T. Schirrmann, M. Schüngel, and S. Dübel. 2011. Targeting antibodies to the cytoplasm. *MAbs.* 3:3–16. https://doi.org/10.4161/mabs.3.1.14110

Marschall, A.L., C. Zhang, A. Frenzel, T. Schirrmann, M. Hust, F. Perez, and S. Dübel. 2014. Delivery of antibodies to the cytosol: debunking the myths. *MAbs.* 6:943–956. https://doi.org/10.4161/mabs.29268

Miyazaki, K. 2011. MEGAWHOP cloning: A method of creating random mutagenesis libraries via megaprimer PCR of whole plasmids. *Methods Enzymol.* 498:399–406. https://doi.org/10.1016/B978-0-12-385120-8.00017-6

Muratoglu, S., S. Georgieva, G. Pápai, E. Scheer, I. Enünlü, O. Komonyi, I. Cserpán, L. Lebedeva, E. Nabirochkina, A. Udvardy, et al. 2003. Two different Drosophila ADA2 homologues are present in distinct GCN5 histone acetyltransferase-containing complexes. *Mol. Cell. Biol.* 23:306–321. https://doi.org/10.1128/MCB.23.1.306-321.2003

Nakade, S., T. Tsubota, Y. Sakane, S. Kume, N. Sakamoto, M. Obara, T. Daimon, H. Sezutsu, T. Yamamoto, T. Sakuma, and K.T. Suzuki. 2014. Microhomology-mediated end-joining-dependent integration of donor DNA in cells and animals using TALENs and CRISPR/Cas9. *Nat. Commun.* 5:5560. https://doi.org/10.1038/ncomms6560

Natale, F., A. Rapp, W. Yu, A. Maiser, H. Harz, A. Scholl, S. Grulich, T. Anton, D. Hörl, W. Chen, et al. 2017. Identification of the elementary structural units of the DNA damage response. *Nat. Commun.* 8:15760. https://doi.org/10.1038/ncomms15760

Ollion, J., J. Cochennec, F. Loll, C. Escudé, and T. Boudier. 2013. TANGO: a generic tool for high-throughput 3D image analysis for studying nuclear organization. *Bioinformatics.* 29:1840–1841. https://doi.org/10.1093/bioinformatics/btt276

Ratz, M., I. Testa, S.W. Hell, and S. Jakobs. 2015. CRISPR/Cas9-mediated endogenous protein tagging for RESOLFT super-resolution microscopy of living human cells. *Sci. Rep.* 5:9592. https://doi.org/10.1038/srep09592

Renaud, E., P. Martineau, and L. Guglielmi. 2017. Solubility characterization and imaging of intrabodies using GFP-fusions. *Methods Mol. Biol.* 1575:165–174. https://doi.org/10.1007/978-1-4939-6857-2_9

Rinaldi, A.S., G. Freund, D. Desplancq, A.P. Sibler, M. Baltzinger, N. Rochel, Y. Mély, P. Didier, and E. Weiss. 2013. The use of fluorescent intrabodies to detect endogenous gankyrin in living cancer cells. *Exp. Cell Res.* 319:838–849. https://doi.org/10.1016/j.yexcr.2013.01.011

Röder, R., J. Helma, T. Preiß, J.O. Rädler, H. Leonhardt, and E. Wagner. 2017. Intracellular delivery of nanobodies for imaging of target proteins in live cells. *Pharm. Res.* 34:161–174. https://doi.org/10.1007/s11095-016-2052-8

Rothbauer, U., K. Zolghadr, S. Tillib, D. Nowak, L. Schermelleh, A. Gahl, N. Backmann, K. Conrath, S. Muyldermans, M.C. Cardoso, and H. Leonhardt. 2006. Targeting and tracing antigens in live cells with fluorescent nanobodies. *Nat. Methods.* 3:887–889. https://doi.org/10.1038/nmeth953

Schermelleh, L., P.M. Carlton, S. Haase, L. Shao, L. Winoto, P. Kner, B. Burke, M.C. Cardoso, D.A. Agard, M.G. Gustafsson, et al. 2008. Subdiffraction multicolor imaging of the nuclear periphery with 3D structured illumination microscopy. *Science.* 320:1332–1336. https://doi.org/10.1126/science.1156947

Schneider, A.F.L., and C.P.R. Hackenberger. 2017. Fluorescent labelling in living cells. *Curr. Opin. Biotechnol.* 48:61–68. https://doi.org/10.1016/j.copbio.2017.03.012

Schnell, U., F. Dijk, K.A. Sjollema, and B.N. Giepmans. 2012. Immunolabeling artifacts and the need for live-cell imaging. *Nat. Methods.* 9:152–158. https://doi.org/10.1038/nmeth.1855

Siddiqui, M.S., M. François, M.F. Fenech, and W.R. Leifert. 2015. Persistent γH2AX: A promising molecular marker of DNA damage and aging. *Mutat. Res. Rev. Mutat. Res.* 766:1–19. https://doi.org/10.1016/j.mrrev.2015.07.001

Snapp, E.L., N. Altan, and J. Lippincott-Schwartz. 2003. Measuring protein mobility by photobleaching GFP chimeras in living cells. Curr. Protoc. Cell Biol. Chapter 21:Unit 21.

Soutoglou, E., M.A. Demény, E. Scheer, G. Fienga, P. Sassone-Corsi, and L. Tora. 2005. The nuclear import of TAF10 is regulated by one of its three histone fold domain-containing interaction partners. *Mol. Cell. Biol.* 25:4092–4104. https://doi.org/10.1128/MCB.25.10.4092-4104.2005

Tantale, K., F. Mueller, A. Kozulic-Pirher, A. Lesne, J.M. Victor, M.C. Robert, S. Capozi, R. Chouaib, V. Bäcker, J. Mateos-Langerak, et al. 2016. A single-molecule view of transcription reveals convoys of RNA polymerases and multi-scale bursting. *Nat. Commun.* 7:12248. https://doi.org/10.1038/ncomms12248

Teng, K.W., Y. Ishitsuka, P. Ren, Y. Youn, X. Deng, P. Ge, A.S. Belmont, and P.R. Selvin. 2016. Labeling proteins inside living cells using external fluorophores for microscopy. *Elife.* 5:e20378. https://doi.org/10.7554/eLife.20378

Teves, S.S., L. An, A.S. Hansen, L. Xie, X. Darzacq, and R. Tjian. 2016. A dynamic mode of mitotic bookmarking by transcription factors. *Elife.* 5:e22280. https://doi.org/10.7554/eLife.22280

Van Regenmortel, M.H. 2014. Specificity, polyspecificity, and heterospecificity of antibody-antigen recognition. *J. Mol. Recognit.* 27:627–639. https://doi.org/10.1002/jmr.2394

van Royen, M.E., A. Zotter, S.M. Ibrahim, B. Geverts, and A.B. Houtsmuller. 2011. Nuclear proteins: finding and binding target sites in chromatin. *Chromosome Res.* 19:83–98.

Vosnakis, N., M. Koch, E. Scheer, P. Kessler, Y. Mély, P. Didier, and L. Tora. 2017. Coactivators and general transcription factors have two distinct dynamic populations dependent on transcription. *EMBO J.* 36:2710–2725. https://doi.org/10.15252/embj.201696035

Wild, T., and P. Cramer. 2012. Biogenesis of multisubunit RNA polymerases. *Trends Biochem. Sci.* 37:99–105. https://doi.org/10.1016/j.tibs.2011.12.001

Ying, Q.L., J. Wray, J. Nichols, L. Batlle-Morera, B. Doble, J. Woodgett, P. Cohen, and A. Smith. 2008. The ground state of embryonic stem cell self-renewal. *Nature.* 453:519–523. https://doi.org/10.1038/nature06968

Zeder-Lutz, G., A. Benito, and M.H. Van Regenmortel. 1999. Active concentration measurements of recombinant biomolecules using biosensor technology. *J. Mol. Recognit.* 12:300–309. https://doi.org/10.1002/(SICI)1099-1352(199909/10)12:5<300::AID-JMR467>3.0.CO;2-N

Zhao, Z.W., R. Roy, J.C. Gebhardt, D.M. Suter, A.R. Chapman, and X.S. Xie. 2014. Spatial organization of RNA polymerase II inside a mammalian cell nucleus revealed by reflected light-sheet superresolution microscopy. *Proc. Natl. Acad. Sci. USA.* 111:681–686. https://doi.org/10.1073/pnas.1318496111